ISSN: 2165-3259

JAOCR

Official Journal of the American Osteopathic College of Radiology

NUCLEAR MEDICINE

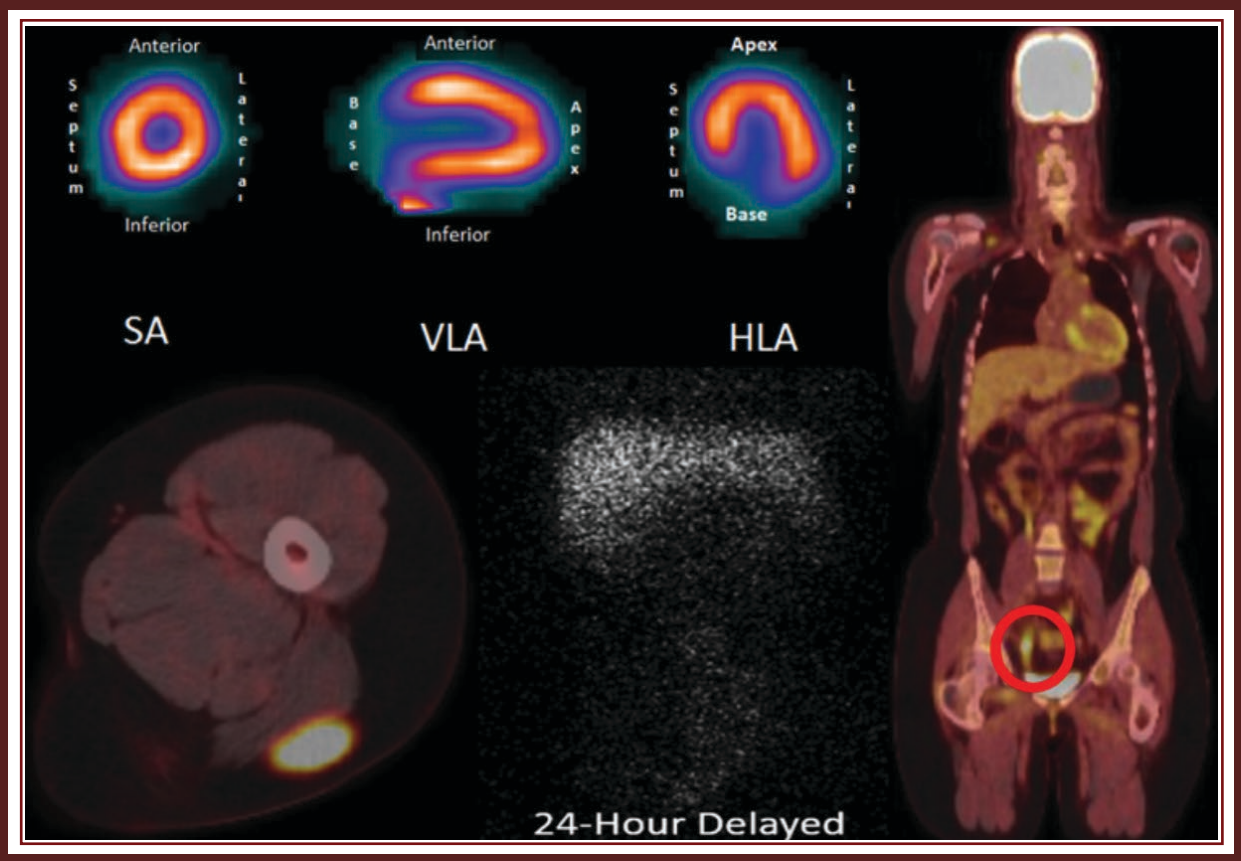

Guest Editor: Ely A. Wolin, M.D.

Editor-in-Chief: William T. O'Brien, Sr., D.O.

July 2016, Vol. 5, Issue 3

JAOCR

Official Journal of the American Osteopathic College of Radiology

Aims and Scope

The Journal of the American Osteopathic College of Radiology (JAOCR) is designed to provide practical up-to-date reviews of critical topics in radiology for practicing radiologists and radiology trainees. Each quarterly issue covers a particular radiology subspecialty and is composed of high-quality review articles and case reports that highlight differential diagnoses and important teaching points.

Access to Articles

All articles published in the JAOCR are open access online. Subscriptions to the journal are not required to view or download articles. Reprints are not available.

Copyrights

Guide for Authors

Submissions for the JAOCR are by invitation only. If you were invited to submit an article and have questions regarding the content or format, please contact the appropriate Guest Editor for that particular issue. Although contributions are invited, they are subject to peer review and final acceptance.

Editor-in-Chief

Associate Editor

Editorial Board

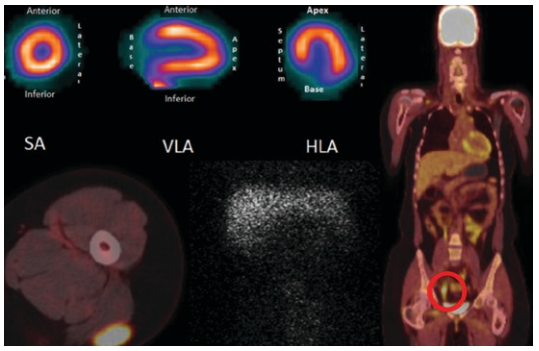

JAOCR

NUCLEAR MEDICINE

Guest Editor: Ely A. Wolin, M.D.

From the Editor

Review Articles

Differential-Based Case Reviews

JAOCR at the Viewbox

"Try not to become a person of success, but rather try to become a person of value."

—Albert Einstein

In this Issue

Ely A. Wolin, M.D.

Chief of Nuclear Medicine, David Grant USAF Medical Center, Travis AFB, CA

I am distinctly honored to have the opportunity to serve as guest editor for a nuclear medicine (NM) edition of the JAOCR. Special thanks to Dr. William O'Brien, editor-in-chief, for entrusting me with such a tremendous opportunity and responsibility.

I was incredibly excited when the opportunity first arose to function as guest editor for this edition—but some trepidation soon followed. Having reviewed past issues, I wanted to ensure we could meet the goal of providing current and relevant information to practicing radiologists and trainees, while upholding JAOCR's high-quality standard. Because of the hard work of the authors, peer reviewers, and editorial staff, I wholeheartedly believe we have accomplished that goal.

Our first review article covers SPECT myocardial perfusion imaging. As the most common nuclear medicine exam, it would be remiss to not include it in an NM subspecialty issue. This review aims to provide a greater understanding of the exam, from indications to image acquisition and interpretation.

The second article is a review of NM genitourinary imaging in native kidneys. This article covers several GU examinations, including dynamic renography, diuretic renography, ACEI renography, and radionuclide cystography. The ability for scintigraphy to image physiology remains useful when evaluating the GU system. A solid understating of radiopharmaceutical properties and study acquisition is required for accurate interpretation, and this review helps meet that need.

The case reports center around hypermetabolic appendiceal activity on PET-CT and bone scan uptake in a radiographically benign-appearing lesion in a child. These reports provide differential-based discussions for the key finding in each case. The Viewbox articles present interesting cases of biliary atresia and a hibernoma.

I would again like to express my gratitude for this amazing opportunity. Thanks to all who made it possible, especially the authors and peer reviewers who dedicated time to this endeavor. Also, a heartfelt thank you to those who read our work. Our sincerest desire is that these articles prove beneficial to you and your practice, and possibly even motivate some to consider a subspecialty career in nuclear medicine.

Review of SPECT Myocardial Perfusion Imaging

Lee Holder, D.O., Steven Lewis, M.D., Erik Abrames, M.D, Ely A. Wolin, M.D.

Department of Radiology, David Grant USAF Medical Center, Travis AFB, CA

Myocardial perfusion imaging (MPI) allows for noninvasive evaluation of coronary artery disease (CAD) by detecting flow-limiting disease and providing risk stratification.[1-3] Despite a recent decline in popularity likely due to changing physician behavior, it remains the most frequently ordered nuclear medicine exam.[4] It is important for any provider reading nuclear medicine studies to have a firm understanding of MPI acquisition and interpretation. This review of single photon emission computed tomography (SPECT) MPI, includes its indications, sensitivity and specificity, radiopharmaceuticals, protocols, and an approach to image interpretation with illustrative cases.

Indications

MPI is performed to evaluate for the presence and severity of CAD by detecting flow-limiting disease, risk-stratifying patients, and assessing and quantifying patient risk. It is most frequently ordered for perioperative cardiovascular evaluation and chest pain.

A meta-analysis has shown that a moderate to large defect on MPI is a positive predictor for postoperative cardiac events, while a normal MPI has high negative predictive value for postoperative myocardial infarction (MI) or cardiac death.[5] The 2014 American College of Cardiology (ACC)/American Heart Association (AHA) guidelines for perioperative cardiovascular evaluation and management of patients undergoing noncardiac surgery is a good reference for perioperative indications.[6] According to these guidelines, exercise testing with cardiac imaging is indicated for preoperative patients with elevated risk and poor or unknown functional capacity, or noninvasive pharmacologic stress testing (dobutamine stress echocardiogram or MPI) in patients with elevated risk and poor (< 4 METs) functional capacity, if the results will change surgical management.[6] MPI also may be indicated in patients with suspected valvular heart disease, as valvular disease increases the cardiac risk associated with noncardiac surgery.[6] Overall, a reversible defect on MPI is a more concerning predictor for perioperative cardiac events, and a fixed defect is a predictor for long-term cardiac events.[6]

The American College of Radiology (ACR) appropriateness criteria is another useful resource for reviewing appropriate study utilization. According to these criteria, SPECT MPI is *usually appropriate* in the clinical setting of chest pain suggestive of acute coronary syndrome in stable patients with no ischemic electrocardiogram (ECG) changes and negative lab markers.[7] A rest-only SPECT has been shown to have a high negative predictive value for acute coronary syndrome during active chest pain, although it is less sensitive than stress SPECT after the pain has resolved.[7,8] SPECT MPI is also *usually appropriate* for use in chronic chest pain with a high probability of CAD,[9] chronic chest pain with a low to intermediate probability of CAD,[10] and in dyspnea with a suspected cardiac origin.[11] The ACR has given a *may be appropriate* grading to the use of SPECT MPI in acute nonspecific chest pain in a setting of low probability of CAD.[12] This is most appropriate when there is a need to exclude CAD as a potential source in the setting of negative cardiac enzymes and negative or equivocal ECG findings. A *usually not appropriate* grade applies to the use in asymptomatic patients with a low to intermediate risk of CAD but a *may be appropriate* grade applies in

Table 1. ACR Appropriateness Criteria

Chronic Chest Pain — High Probability of Coronary Artery Disease	9
Chronic Chest Pain — Low to Intermediate Probability of Coronary Artery Disease	8
Dyspnea — Suspected Cardiac Origin	7
Chest Pain Suggestive of Acute Coronary Syndrome	7
Acute Nonspecific Chest Pain—Low Probability of Coronary Artery Disease	6
Asymptomatic Patient at Risk for Coronary Artery Disease: Low, Intermediate, and High Risk	1, 2, 5

Rating: 1-3 Usually Not Appropriate, 4-6 May Be Appropriate, 7-9 Usually Appropriate

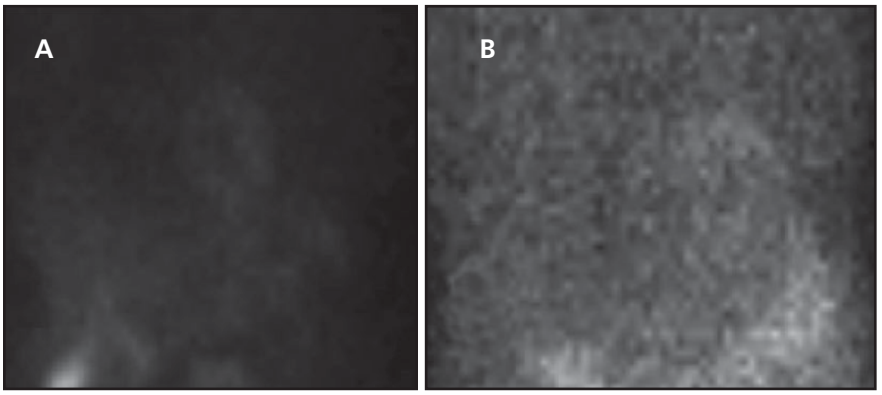

FIGURE 1. *Representative raw data images from MPI using Tc99m-tetrofosmin (A) and Tl-201 (B) showing the improved statistics with the Tc99m-based agents. Tl-201 images have decreased signal-to-noise due to low-energy photons, which are more likely to be attenuated and require lower dosages for radiation protection.*

asymptomatic patients with a high risk of CAD.[13] **Table 1** is a brief review of these guidelines.

The ACC Foundation Appropriate Use Criteria Task Force, along with other subspecialty groups, performed an appropriate use review for multiple categories of stable ischemic heart disease, which is another helpful resource but out of the scope of this review article.[14]

SPECT Sensitivity and Specificity

Coronary angiography remains the gold standard for CAD evaluation. A large meta-analysis study published in 2012 compiling data from 2000-2010 that compared SPECT MPI, positron emission tomography (PET) and cardiac MR (CMR) found MPI has overall sensitivity of 88% and specificity of 61% for diagnosing obstructive CAD.[15] Sensitivity was similar to PET and CMR but MPI has lower specificity. MPI remains more widely used than PET and CMR, and can be used in patients in whom other modalities are limited.[16]

Quantification software was developed to assist with MPI interpretation that allows for quantified risk stratification. Such software, discussed more below, compares patient perfusion to a database of normals and provides quantification of the differences expressed as summed stress score (SSS), summed rest score (SRS) and summed difference score (SDS). According to one study, SSS ≤ 3 carries a 0.9% annual risk for cardiac mortality vs. 5% for SSS > 12.[17]

One area of low sensitivity for SPECT MPI is balanced or multivessel ischemia. This is due to the assumption that the best perfused areas are normal, leading to diffuse normalization of diffuse decreased perfusion. Increased pulmonary uptake, right ventricular (RV) uptake, decline in left ventricular (LV) ejection fraction (EF) with stress, and transient ischemic dilation (TID) are indicators of possible balanced multivessel disease.[16,17]

Radiopharmaceuticals

Historically, thallium-201 (Tl-201) was used in nuclear medicine to image the myocardium. Tl-201 is a potassium analogue that decays primarily via electron capture to mercury-201 emitting 69-81 KeV x-rays.[18] It is actively transported into myocardial cells by sodium-potassium pumps. Thallium uptake is directly proportional to perfusion of the myocardial cells. After initial distribution, Tl-201 redistributes throughout the myocardium as a result of cellular washout and continued cellular uptake. Ischemic regions of myocardium demonstrate delayed washout, but eventually equalize with the remainder of the myocardium. Regions that do not show redistribution are considered fixed defects. With a relatively long 73-hour half-life, Tl-201 is administered in low dosages, 1.5-2.0 mCi at both rest and stress.[19] With such low dosage and low energy photons, Tl-201-based imaging produces counting statistics inferior to those provided by newer agents, which have mostly replaced thallium for MPI (**Figure 1**). Tl-201 remains useful in viability imaging. Twenty-four-hour delayed redistribution into a fixed defect suggests viable, hibernating myocardium, which may respond to revascularization.

Technetium 99m (Tc99m)-based agents are primarily used for SPECT MPI now. It is well-known that the 140 KeV photopeak from Tc-99m isomeric transition is ideal for gamma camera imaging. For perfusion studies, the primary agents bound to Tc99m are tetrofosmin and sestamibi. Both agents are lipophilic and, therefore, enter myocardial cells by passive diffusion in a quantity directly proportional to blood flow. There they bind to proteins within mitochondria via electrostatic interactions.[20] When a myocyte is damaged, these electrostatic interactions occur in much smaller numbers, resulting in far lower accumulation and reduced counts.[20]

Both sestamibi and tetrofosmin demonstrate efficient myocardial uptake without significant physiologic redistribution.[18] Both also underestimate myocardial blood flow at stress, beginning when blood flow reaches approximately double baseline.[18] Because a radiopharmaceutical is primarily removed from the myocardium by blood flow, a larger dose is required at stress when blood flow is higher to maintain adequate counts.[18,21] Tetrofosmin has less hepatic uptake and faster hepatic clearance.[18] Tetrofosmin is thus preferred with pharmacologic stress, as hepatic uptake is greater than with exercise.[22]

Recommended dosage for sestamibi is 10 mCi at rest imaging and 30 mCi at stress, and 5-12 mCi at rest, 15-33 mCi at stress with tetrofosmin. There are no provided dose adjustments for either agent in pediatric or geriatric patients, or in patients with metabolic impairment.[23,24] Estimated effective radiation dose for myocardial perfusion imaging studies is 9-11 mSv for a 1-day Tc99m-based study compared to 20 mSv for a Tl-201 study.[25]

Stress Protocols

Before any stress test, the patient should be NPO for 4 to 6 hours to reduce blood flow to the bowel and liver. Calcium channel blockers and beta-blockers should be discontinued for 48-72 hours, and long-acting nitrates discontinued for 12-24 hours. Caffeine should not be consumed for 1 day prior to the exam.[18] Myocardial stress is achieved either with an exercise treadmill test (ETT) or pharmacologic agents.

ETT involves a multistage exercise test based on a Bruce or modified Bruce protocol, during which the speed and grade of the treadmill are gradually increased. The modified Bruce protocol starts with no slope, vs. 10% for the Bruce protocol, and the speed and slope are increased at a slower rate. The patient must achieve a heart rate of at least 85% of their predicted maximum heart rate (220 beats/minute [min] minus the patient's age) for an ETT to be adequate. The radiopharmaceutical is injected at peak stress and the patient should continue to exercise for an additional minute.

Pharmacologic stress can be used if the patient is unable to perform exercise or an ETT must be terminated before the patient's heart rate reaches 85% of the maximum predicted. Other indications for a pharmacologic stress test include acute coronary syndrome, hypotension, a left bundle branch block (LBBB), or severe congestive heart failure. A patient with LBBB may have false positive results from an exercise stress test, typically an artifactual septal defect.

Non-nitrate vasodilators such as dipyridamole, adenosine, and regadenoson can be used for pharmacologic stress. The resultant vasodilation, typically 3 to 5 times baseline, tests coronary flow reserve.[26] Minor side effects are common and include flushing, headache and dyspnea. Regadenoson (Lexiscan) is the most frequently used agent. It is a selective A2A receptor agonist that results in coronary vasodilation with fewer side effects, injected as a 400μg bolus over 10 seconds.[26] Non-nitrate vasodilators should not be used in patients with second- or third-degree heart block. Caution should also be used in patients with reactive airway disease as these agents can cause severe bronchospasm.

Dobutamine has also been used as a pharmacologic stress agent. Dobutamine is a synthetic catecholamine that acts on alpha- and beta-adrenergic receptors, which increase cardiac work through positive inotropic and chronotropic effects. Dobutamine can be used as an alternative to vasodilator therapy in cases of severe asthma. Initial infusion dose is 5 ug/kg/min over 3 min. The infusion is then increased to 10 μg/kg/min for another 3 minutes. The infusion rate can be increased to a maximum of 40 μg/kg/min every 10 minutes.[26] The radiopharmaceutical is then injected 1 minute after the maximum tolerable dose. Frequent side effects include chest pain and arrhythmias.

Imaging Protocol

Due to the physiologic redistribution of Tl-201, imaging starts with the stress portion of the examination. While Tl-201 can be injected at both stress and rest, many will use a single injection protocol. This entails an injection of around 4 mCi of Tl-201 at peak myocardial stress with the poststress images obtained as soon as heart rate returns to normal. If the stress images are abnormal, redistribution images are obtained around the 4-hour mark. Viability images can be obtained at 24 hours if there is a fixed defect, and determination of viability will assist clinical management.

With the Tc99m-based mitochondrial imaging agents, the primary options are using either a 1 or 2-day protocol. The 1-day protocol is primarily used, as it is more convenient for patients and more efficient. The 2-day protocol allows for higher administered dosage at rest, which can be advantageous particularly in obese patients, and offers the possibility of stress-only imaging.

The 1-day protocol involves obtaining a rest study and a stress study on the same day. The patient receives 2 doses of radiopharmaceutical approximately 1.5 to 2 hours apart.[26] The rest study is performed first with images obtained generally 30 to 60 minutes after injection of 8-10 mCi of Tc-99m sestamibi or tetrofosmin. After 1.5 to 2 hours, allowing sufficient clearance of the rest dose, the patient undergoes the stress portion of the study. During peak stress a second dose of radiopharmaceutical is administered, typically 25 to 30 mCi. The patient is then imaged quickly (15-20 min) after radiopharmaceutical administration. The larger second dose provides higher quality images, generally favored with the stress portion of the examination, especially for gated images.

In large patients, a small dose of radiopharmaceutical can result in poor image quality and nondiagnostic images due to increased attenuation. In these cases, a 2-day protocol can be used to allow for higher administered activity for both the rest and stress portions.[26]

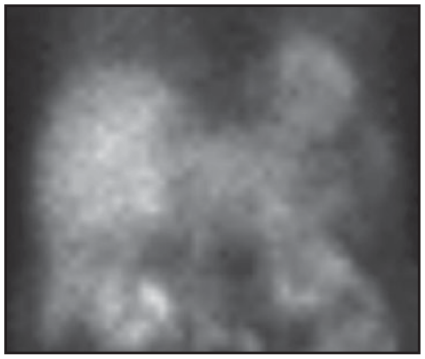

FIGURE 2. *Raw data image from MPI showing lack of gallbladder uptake. Follow-up ultrasound and hepatobiliary scan were consistent with acute cholecystitis.*

The larger doses must be separated by a day to ensure counts originate from the desired injection. For a 2-day protocol, the stress portion is performed on the first day. The Tc-99m radiopharmaceutical is injected at peak stress and the patient is imaged quickly (15-20 min). If the stress portion of the study is normal, no further imaging is necessary. If the stress portion of the study is abnormal, the patient returns the next day to receive of a second dose of Tc-99m radiopharmaceutical at rest with images obtained 30-60 min after injection.

SPECT imaging can utilize either a 180° or 360° acquisition, with 32 or 64 stops or continuous acquisition. For nonattenuation-corrected imaging, 180° is preferred. The patient is usually supine, unless using a dedicated cardiac chair, with arms up to position outside the field of acquisition. Prone imaging can be helpful for patients with a lot of attenuation. The use of attenuation correction is occasionally essential, such as in patients with recent pacemaker placement who cannot put their arm up out of the field of view. If attenuation correction is used, it is imperative to evaluate both the corrected and uncorrected data as the correction software can create artifactual perfusion defects.

Interpretation

The interpretation of SPECT MPI includes four broad categories: raw data, qualitative analysis, quantitative analysis, and evaluation of motion and function.

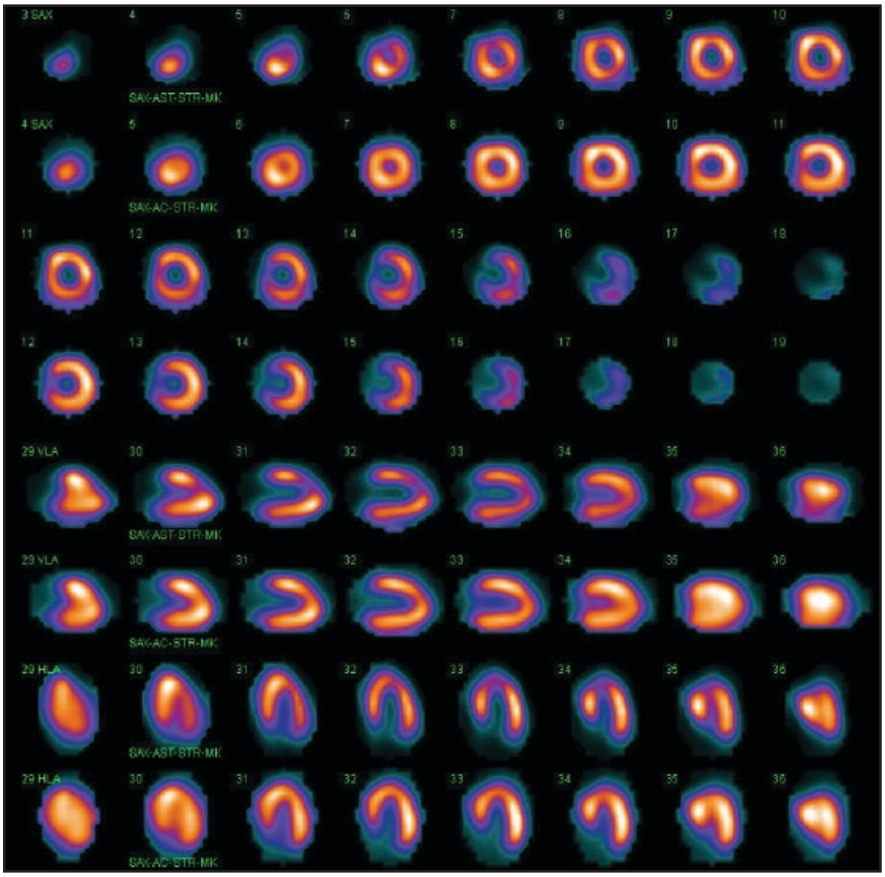

FIGURE 3. *Nonattenuation-corrected (top row) and attenuation-corrected (bottom row) images from an MPI SPECT CT showing a small mild-to-moderate severity distal anteroseptal defect that resolves with attenuation correction and is attributable to breast attenuation.*

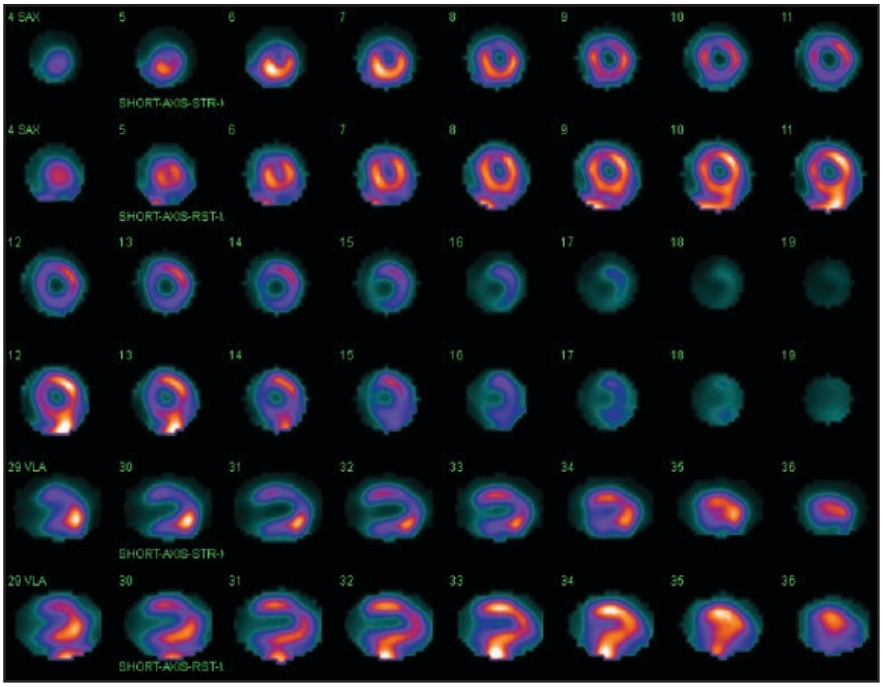

FIGURE 4. *SA and VLA images from a SPECT MPI shows GI activity adjacent to the heart on the rest images, with GI counts seen joining the inferior wall.*

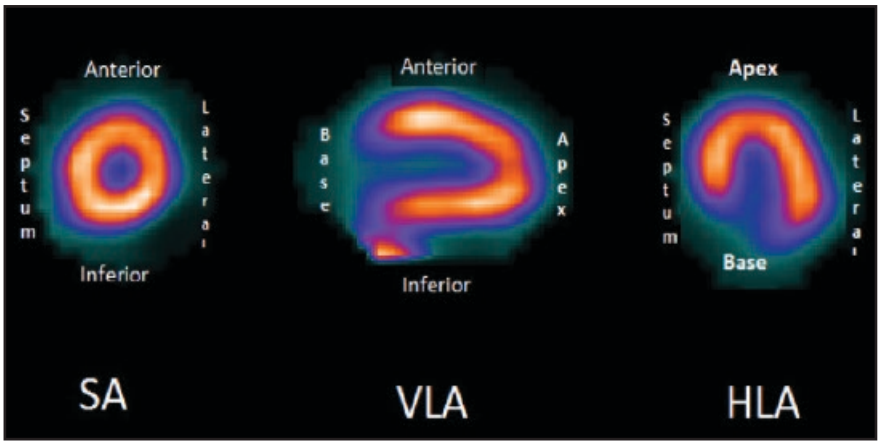

FIGURE 5. *Representative short axis (SA), vertical long axis (VLA) and horizontal long axis (HLA) images with the left ventricular walls labeled.*

Raw data images are generally viewed as rotating cinematic (cine) images. These images allow the interpreter to evaluate radiotracer distribution, and assess for attenuation, motion or interfering splanchnic activity. Normal physiologic distribution of the Tc-99m-based mitochondrial imaging agents includes activity within the heart, liver, gallbladder, small bowel, kidneys, bladder and sometimes the stomach. Mild uptake may be seen within the lungs and skeletal muscle as well, particularly if an exercise stress protocol is used. Uptake within the RV is normal, especially on stress imaging; however, if RV activity approaches the left, it is abnormal and may indicate RV strain. Any uptake outside of these normal structures requires attention. Particular attention should be paid to the axillary nodes and breast tissue, as the mitochondrial agents are nonspecific tumor imaging agents. In fact, Tc99m-sestamibi is used for breast-specific gamma imaging. Any breast uptake should be correlated with mammography. Uptake in the axillary nodes is often from radiopharmaceutical extravasation at the injection site, but can be seen with metastatic disease and may warrant further workup. A right upper quadrant ultrasound should be recommended if there is no uptake within the gallbladder in a patient without prior cholecystectomy (**Figure 2**).

Identifying attenuation on the raw cine images may aid problem-solving for defects noted during qualitative analysis. It is particularly helpful to note whether a shift in attenuation occurs between the rest and stress images as this may result in an artifactual reversible defect. Breast tissue leads to attenuation on most female patients, usually resulting in an anteroseptal defect on qualitative review. The diaphragm and lateral chest wall also frequently attenuate, resulting in defects involving the inferior base of the heart. Also, the interpreter should be aware of external devices such as pacemakers that may overlie portions of the heart and mimic perfusion defects. SPECT computed tomography (CT) can be helpful as the CT component allows for attenuation correction of the SPECT data (**Figure 3**). At our institution, we perform the examination as a SPECT CT if the patient has a high BMI or is unable to raise both arms above the head. Repeating the stress images in the prone position is also sometimes helpful, as a true perfusion defect will not shift.

Motion correction should be applied during image processing if there is significant motion. Assessment after correction should show no significant cardiac motion.

Splanchnic activity projecting adjacent to the heart—usually bowel or hepatobiliary activity—may limit evaluation. This "gut crosstalk" (**Figure 4**) usually affects the inferior wall. The high activity within the adjacent organs may either artificially add or subtract counts from the myocardium. Falsely elevated counts can mask a true defect, while falsely decreased counts can create a false defect.[3] Prone positioning may increase distance between abdominal viscera and the heart, possibly limiting gut crosstalk, and adding a small exercise component to pharmacologic stress may decrease splanchnic activity. The most important way to limit gut crosstalk is to allow sufficient time before imaging to allow activity to clear.[3] At some facilities, patients drink a carbonated beverage prior to imaging to help clear gastric activity.

The raw SPECT data is processed to create image slices that are parallel and perpendicular to the long axis of the heart for qualitative analysis. The horizontal long axis (HLA) is parallel to the inferior wall giving the best view of the septum and lateral wall; the vertical long axis (VLA) is parallel to the septum giving the best view of the anterior and inferior walls; the short axis (SA) is perpendicular to the long axes and parallel to the base (**Figure 5**). Evaluating these images for perfusion abnormalities provides the primary information clinicians need. The poststress data is the most important. If the stress data is normal, there is no evidence of ischemia or infarct. The primary purpose of rest images is to provide specificity to a stress defect. The images can be evaluated using multiple color schemes, each of which comes with an inherent associated sensitivity and specificity. Determining the color scheme is a personal preference, but requires an understanding of the statistics associated with the choice.

If present, stress perfusion defects are described by size, severity, location, extent and reversibility. Size is the amount of LV myocardium involved, described as small, moderate or large, equating to < 10%, 10% to 20%, or > 20% of myocardium. Severity is described by the percentage of counts compared to the most active area of myocardium. As the images are normalized to the "hottest" pixel, this is one of the ways "gut crosstalk" can affect interpretation. Masking the data to exclude extra-cardiac activity

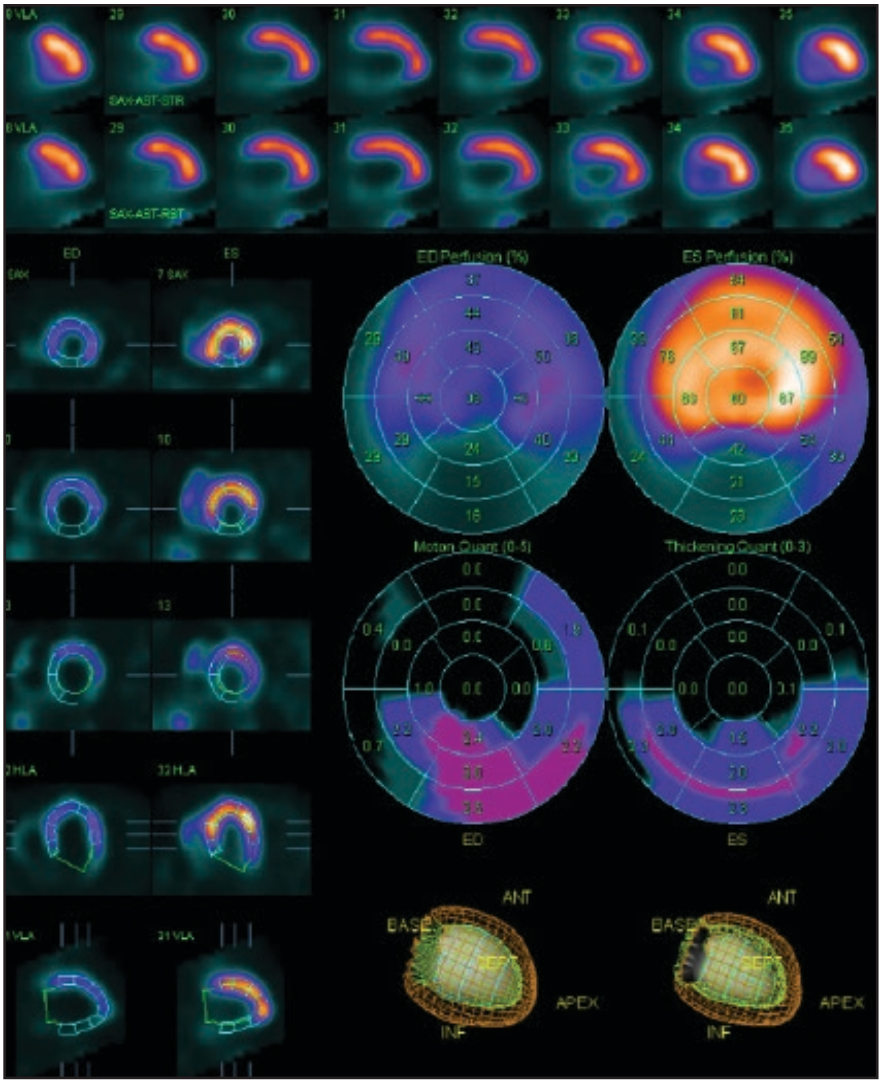

FIGURE 6. *Inferior wall infarct on MPS. VLA images show a large severe perfusion defect involving the entire inferior wall with associated abnormal wall motion and thickening on gated analysis.*

Table 2. Comparison of ischemia, stunned myocardium, hibernating myocardium and infarct.

	Rest Perfusion	Stress Perfusion	Wall Motion	Viability
Ischemia	Normal	Defect	Mostly Normal	Viable
Stunned Myocardium	Norrmal	Normal	Hypokinetic to Akinetic	Viable
Hibernating Myocardium	Defect	Defect	Hypokinetic to Akinetic	Viable
Infarct	Defect	Defect	Akinetic	Non-Viable

Findings seen on rest and stress imaging on SPECT along with wall motion and expected findings on corresponding viability study.

can help, but it is impossible to exclude activity immediately adjacent to the heart without losing real data. At our institution, anything visibly within 75% to 100% of the hottest pixel is considered normal. Mild decrease is 50% to 75%, moderate is 25% to 50%, and severe is between 0% to 25%, with 0% considered complete. Location refers to the ventricular segments/walls involved, and extent describes which slices within the segment are involved, typically broken down into base, mid slices, distal/apical slices and apex. Rest images are needed to determine reversibility, which in turn, determines the primary differential. When evaluating for reversibility, it is imperative to ensure that the rest and stress data are similarly aligned.

An example description of a perfusion defect could be, "a small, mild severity anterior wall perfusion defect extending from mid slices through the apex that is reversible."

A fixed defect is a perfusion defect present at stress and rest. Primary differential for a fixed defect includes scarring from infarction, chronically ischemic areas called hibernating myocardium, or attenuation. Attenuation defects generally are worse at rest than stress (because approximately 3 times the dosage is given at stress with a 1-day protocol), are in a distribution that matches known areas of attenuation, should be seen on the raw images, and will have normal motion. Infarction and hibernating myocardium will look identical on SPECT MPI (**Figure 6**). A separate viability study can differentiate, if it is clinically necessary, as hibernating myocardium will respond to revascularization (**Table 2**).

A poststress perfusion defect that improves at rest is called reversible, and is concerning for stress-induced ischemia (**Figure 7**). As discussed, shifting attenuation leading to an area of myocardium being attenuated on the poststress images but not the rest images is a possible cause for a false positive. Ensuring the defect matches a vascular distribution and thorough evaluation of the raw data can help prevent this pitfall. SPECT-CT with attenuation correction is also an

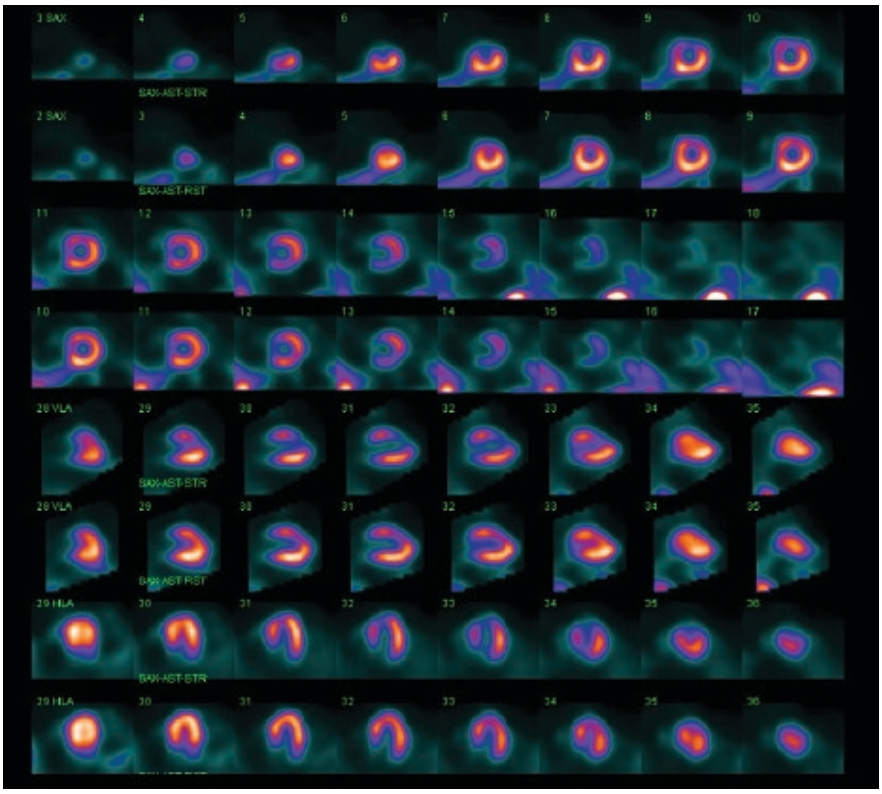

FIGURE 7. *SPECT MPI showing a large severe mid-to-distal anterior wall and apical stress perfusion defect that shows reversibility at rest. Subsequent cardiac catheterization showed high-grade (approximately 90%) stenosis in the left anterior descending artery proximal to a previously placed stent.*

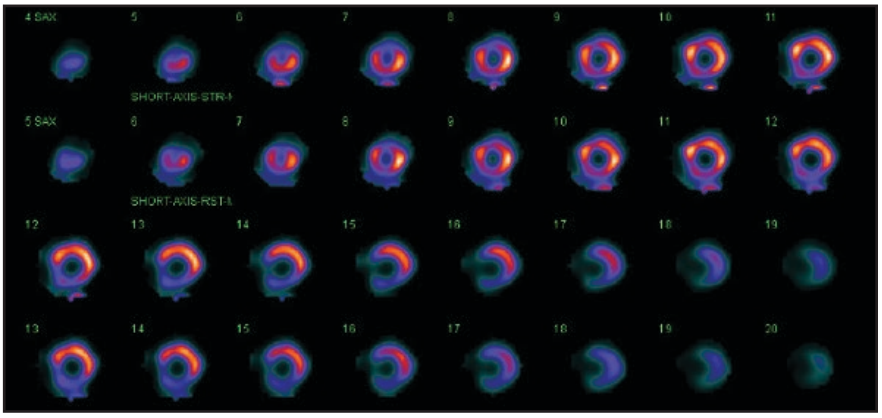

FIGURE 8. *SA images from SPECT MPI show a small moderate distal anterior stress perfusion defect that is centrally fixed with reversibility along the margins, suggesting infarct with peri-infarct ischemia.*

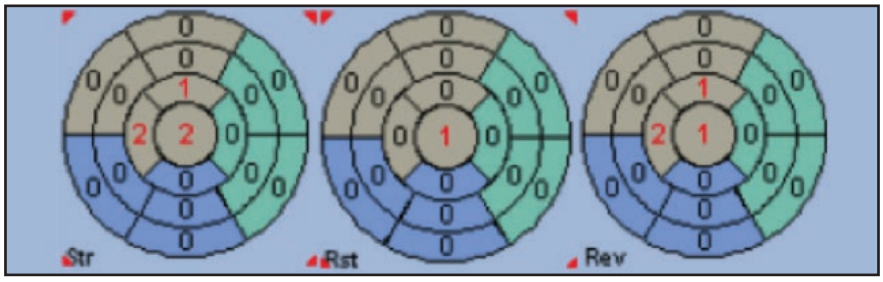

FIGURE 9. *Seventeen segment polar map images from SPECT MPI showing an SSS of 5, SRS of 1, and SDS of 4, with quantitative ischemia in the distal/apical septal segment.*

option. Areas of reversibility within a mostly fixed defect should be reported as such. An example is a fixed defect with reversibility along the margins representing an infarct with peri-infarct ischemia (**Figure 8**).

Computer software can help provide quantitative analysis of myocardial perfusion. Most programs use a 17-segment polar map of the LV to help identify specific areas of perfusion abnormality. The images are compared to a normalized control database. A 0-4 scoring system is used for each segment, with 0 being normal and 1-4 given for mildly decreased to completely absent counts. This scoring applies to both stress and rest data, and the numbers in each polar map are added to provide the SSS and SRS. SSS can help assess patient risk of a significant cardiac event. SSS of ≤ 3 is normal, 4-7 is low risk, 8-12 is intermediate risk, and ≥ 13 is high risk.[21] The SDS is assessed by subtracting the SRS from the SSS. Any segment with an SDS of ≥ 2 is considered reversible and concerning for ischemia (**Figure 9**). We typically give more weight to our qualitative analysis if the quantitative results are discordant, as the quantitative data relies on appropriate contouring and is easily manipulated.

As previously noted, TID may be a sign of balanced multivessel ischemia. The term is somewhat of a misnomer as there is no actual dilation, especially as the stress images are usually not obtained until the patient has returned to resting physiology. The apparent dilation is likely due to diffuse subendocardial hypoperfusion, which can be seen with multivessel CAD, hypertensive heart disease and dilated cardiomyopathy (**Figure 10**). The TID ratio compares the apparent stress chamber size to the rest chamber. We use a cutoff of 1.22 for ETT and 1.32 for pharmacologic stress, at or above which is abnormal.[27]

With the addition of gated images, LV motion and function can be analyzed. We only obtain gated images poststress, as the statistics are better due to the higher administered activity, and the patient is already physiologically

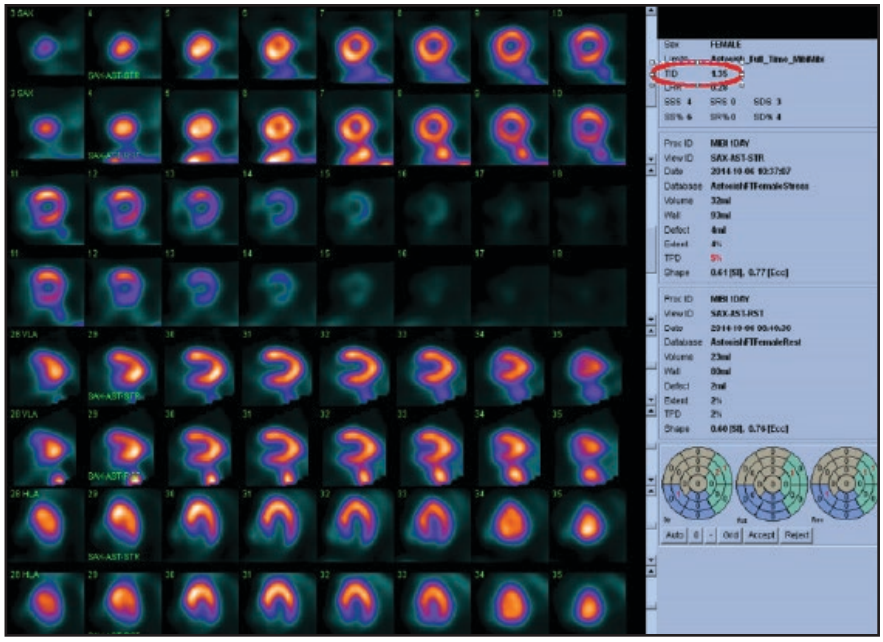

FIGURE 10. *SA, VLA and HLA images show apparent dilation of the left ventricular cavity on the stress images with a TID ratio of 1.35 (red circle).*

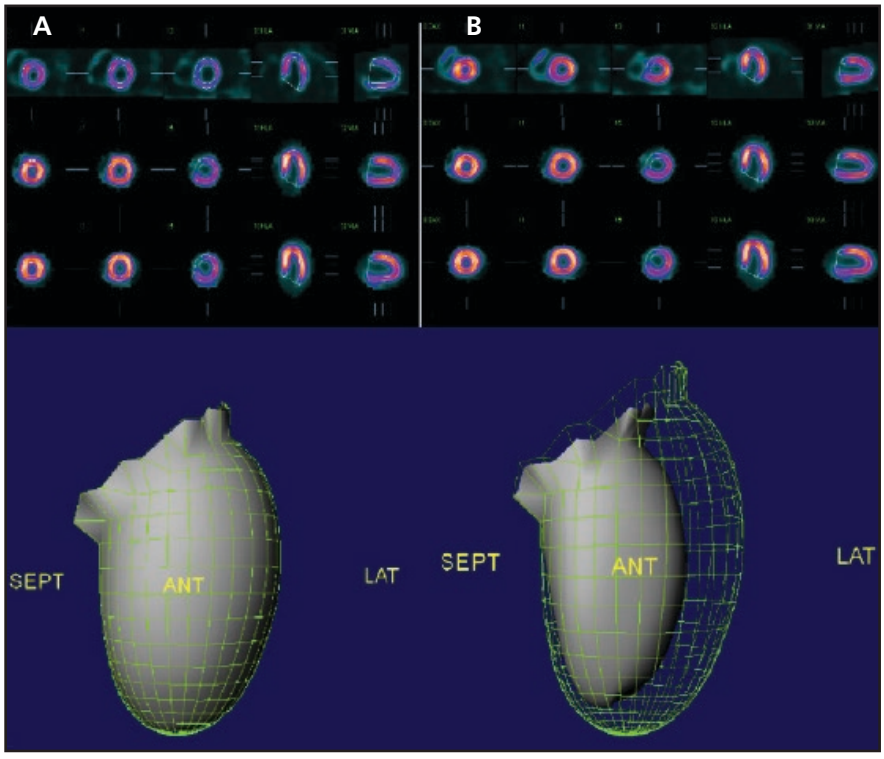

FIGURE 11. *Top row gated slice images in diastole (A) and systole (B) show normal thickening and brightening of the septum, which on 3D-surface-rendered images appears akinetic.*

at rest at the time of acquisition. Normal LV motion results in at least 20% shortening of the long axis and 40% shortening along the short axis, with the anterior wall moving the most and the apex moving the least.[18] The septum should thicken and move toward the center. Cine analysis of slices from the 3 axes of the gated images should show all walls thickening and brightening with systole. The basal one-third of the septum is membranous and should not be mistaken for a defect or motion abnormality. Apical thinning, which is anatomically normal, may also mimic a defect. If wall motion is normal, the ventricle thickens normally, and a small defect is evident on rest and stress views, it is likely normal.[21] Most software will also create a 3D map of the left ventricle, highlighting the extrapolated chamber throughout the cardiac cycle.

Wall motion is either normal, hypokinetic, akinetic, or dyskinetic. Hypokinesis can be seen with areas of ischemia if the patient has not fully recovered from stress. Akinesis is usually associated with infarction or hibernating myocardium. Dyskinesis, outward movement during systole, suggests aneurysm formation at the site of transmural infarction.

After coronary artery bypass grafting (CABG), anteromedial deviation of the heart—commonly referred to as post-CABG kinetics—can be seen due to interruption of the normal fascial bands. The 3D renderings of the chamber will resemble septal hypo- or akinesis, but review of the slices will show the septum normally thickening and increasing in counts (**Figure 11**). A "septal bounce," or paradoxical movement of the septum inward during diastole, is nonspecific but may appear with LV restriction (constrictive pericarditis, tamponade, or restrictive cardiomyopathy) or with LBBB (**Figure 12**). If no LBBB is seen on ECG, further analysis is in order. Calculated LVEF is usually provided, with 50% to 70% being normal. This is not as accurate as radionuclide ventriculography.

Summary

SPECT MPI remains a widely used modality to analyze myocardial perfusion. It is particularly useful in identifying flow-limiting stenoses and for risk stratification. Use of appropriate protocols and radiopharmaceutical dosage is paramount in obtaining diagnostic quality images. An ideal approach to image interpretation includes evaluation of raw data, qualitative

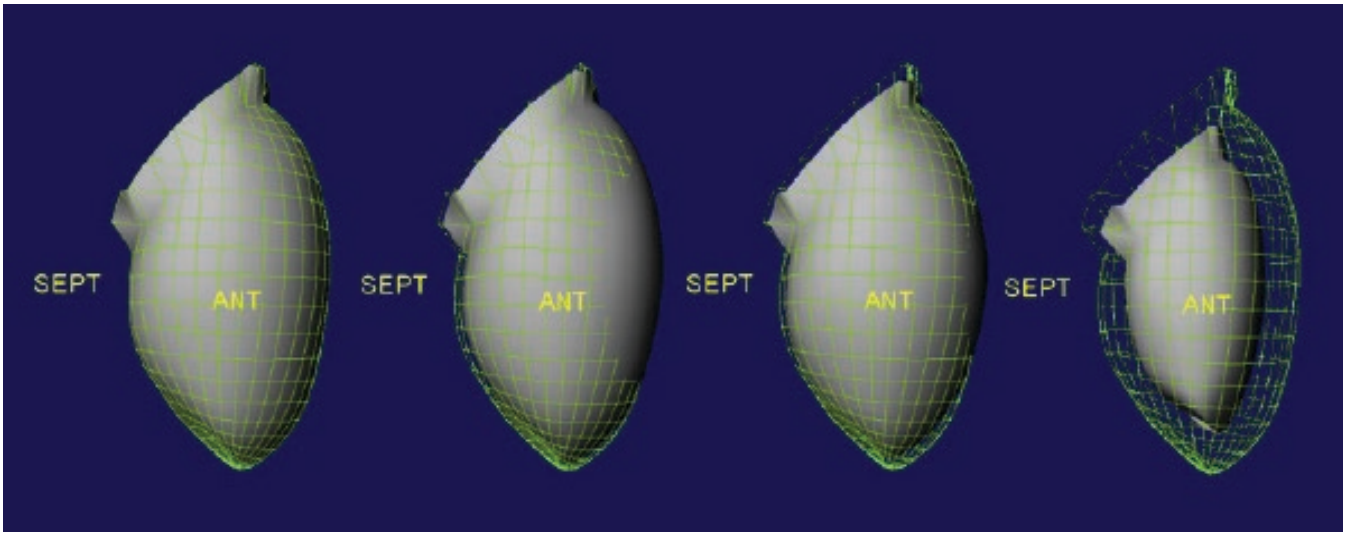

FIGURE 12. *Representative 3D-rendered gated images show paradoxical inward motion of the septum during diastole or, a "septal bounce," in a patient with known LBBB.*

analysis, quantitative analysis, and cardiac motion and function. Accurate interpretation requires a working knowledge of radiopharmaceutical biodistribution, cardiac physiology, as well as common pathologies, pitfalls, and artifacts.

References

1. Ben-Haim S, Murthy VL, Breault C, et al. Quantification of myocardial perfusion reserve using dynamic SPECT imaging in humans: a feasibility study. J Nucl Med 2013;54:873-879.
2. Slomkaa P, Xua Y, Bermana D, et al. Quantitative analysis of perfusion studies: strengths and pitfalls. J Nucl Cardiol 2012;19(2):338-346.
3. Burrell S, MacDonald A. Artifacts and pitfalls in myocardial perfusion imaging. J Nucl Med Technol 2006;34:193-211.
4. McNulty EJ, Hung Y, Almers LM, et al. Population trends from 2000-2011 in nuclear myocardial perfusion imaging use. JAMA 2014;12:1248-1249.
5. Harafuji K, Chikamori T, Kawaguchi S, et al. Value of pharmacologic stress myocardial perfusion imaging for preoperative risk stratification for aortic surgery. Circ J 2005;69:558-563.
6. Fleisher LA, Fleischmann KE, Auerbach AD, et al. 2014 ACC/AHA Guideline on Perioperative Cardiovascular Evaluation and Management of Patients Undergoing Noncardiac Surgery: Executive Summary. J Am Coll Cardiol 2014:64(22)e77-e137.
7. Mammen L, Abbara S, Dorbala S, et al. American College of Radiology ACR Appropriateness Criteria. Chest pain suggestive of acute coronary syndrome. https://acsearch.acr.org/docs/69403/Narrative/. American College of Radiology. Accessed February 17, 2016.
8. Uliel L, Mellnick VM, Menias CO, et al. Nuclear medicine in the acute clinical setting: indications, imaging findings, and potential pitfalls. RadioGraphics 2013;33:375-396.
9. Earls JP, White RD, Woodard PK, et al. Chronic chest pain—high probability of coronary artery disease. https://acsearch.acr.org/docs/69405/Narrative/. American College of Radiology. Accessed February 17, 2016.
10. Woodard PK, White RD, Abbara S, et al. Chronic chest pain—low to intermediate probability of coronary artery disease. https://acsearch.acr.org/docs/69337/Narrative/. American College of Radiology. Accessed February 17, 2016.
11. Abbara S, Ghoshhajra B, White RD, et al. Dyspnea—suspected cardiac origin. https://acsearch.acr.org/docs/69407/Narrative/. American College of Radiology. Accessed February 17, 2016.
12. Hoffmann U, Akers SR, Brown RKJ, et al. Acute nonspecific chest pain—low probability of coronary artery disease. https://acsearch.acr.org/docs/69401/Narrative/. American College of Radiology. Accessed February 17, 2016.
13. Earls JP, Woodard PK, Abbara S, et al. Asymptomatic patient at risk for coronary artery disease. https://acsearch.acr.org/docs/3082570/Narrative/. American College of Radiology. Accessed February 17, 2016.
14. Wolk MJ, Bailey SR, Doherty JU, et al. ACCF/AHA/ASE/ASNC/HFSA/HRS/SCAI/SCCT/SCMR/STS 2013 multimodality appropriate use criteria for the detection and risk assessment of stable ischemic heart disease: a report of the American College of Cardiology Foundation Appropriate Use Criteria Task Force, American Heart Association, American Society of Echocardiography, American Society of Nuclear Cardiology, Heart Failure Society of America, Heart Rhythm Society, Society for Cardiovascular Angiography and Interventions, Society of Cardiovascular Computed Tomography, Society for Cardiovascular Magnetic Resonance, and Society of Thoracic Surgeons. J Am Coll Cardiol 63(4):380-406.
15. Jaarsma C, Leiner T, Bekkers SC, et al. Diagnostic performance of noninvasive myocardial perfusion imaging using single-photon emission computed tomography, cardiac magnetic resonance, and positron emission tomography imaging for the detection of obstructive coronary artery disease: a meta-analysis. J Am Coll Cardiol 2012; 59:1719-1728.
16. Murthy VL, Di Carli MF. Non-invasive quantification of coronary vascular dysfunction for diagnosis and management of coronary artery disease. J Nucl Cardiol 2012;19:1060-1072.
17. Hage FG, Aljaroudi WA. Review of cardiovascular imaging in The Journal of Nuclear Cardiology in 2014: Part 2 of 2: Myocardial perfusion imaging. J Nucl Cardiol 2015;22:714-719.
18. Mettler FA, Guiberteau MJ. Essentials of Nuclear Medicine Imaging 6th Edition. Philadelphia: Elsevier; 2012.
19. Bailey IK, Griffith LS, Rouleau J, Strauss HW, Pitt B. Thallium-201 myocardial perfusion imaging at rest and during exercise. Circulation 1977;55(1):79-87.
20. Husain SS. Myocardial perfusion imaging protocols: is there an ideal protocol? J Nucl Med Technol 2007;35:3-9.
21. Dvorak RA, Brown RKJ, Corbett JR. Interpretation of SPECT/CT myocardial perfusion images: common artifacts and quality control techniques. RadioGraphics 2011;31:2041-2057.
22. Tc-99m sestamibi/tetrofosmin stress-rest myocardial perfusion scintigraphy. University Health Shreveport. http://www.sh.lsuhsc.edu/raddept/pdf/sec18/Rad%20Proc%2018.8.5.5.pdf. Accessed February 20, 2016.
23. Cardiolite kit for the preparation of technetium tc99m sestamibi for injection. Lantheus Medical Imaging. http://www.cardiolite.com. Accessed February 20, 2016.
24. Myoview 30 mL kit for the preparation of Tc99m tetrofosmin for injection. GE Healthcare. Medi-Physics, Inc. http://www3.gehealthcare.com. Accessed February 20, 2016.
25. DePuey, GE. Standard myocardial perfusion spect protocols and associated patient radiation doses. Image Wisely, ACR November 2012.
26. Ziessman HA, O'Malley JP, Thrall JH, Fahey FH. Nuclear Medicine: The Requisites. 4th Edition. Philadelphia: Elsevier; 2014.
27. Golzar Y, Olusanya A, Pe N, et al. The significance of automatically measured transient ischemic dilation in identifying severe and extensive coronary artery disease in regadenoson, single-isotope technetium-99m myocardial perfusion SPECT. J Nucl Cardiol 2015;22(3):526-534.

Disclaimer: The views expressed in this article are those of the author and do not necessarily reflect the official policy or position of the Department of the Air Force, Department of Defense, or the U.S. Government.

Nuclear Medicine Genitourinary Imaging in Native Kidneys

Brian F. McQuillan, M.D., Scott Zelasko, M.D., Ely A. Wolin, M.D.

Department of Radiology, David Grant USAF Medical Center, Travis AFB, CA

Similar to other facets of nuclear medicine, scintigraphic imaging of the genitourinary system emphasizes physiology over anatomy, which is typically evaluated with either ultrasound, computed tomography, or MRI. Nuclear medicine studies catered toward the genitourinary system in nontransplant patients assess renal blood flow, evaluate renal function, identify mechanical or functional obstruction, evaluate for renovascular hypertension, and assess vesicoureteral reflux. This article will review the most common radiopharmaceuticals and their clinical applications in evaluating the genitourinary system in native, nontransplant kidneys.

The kidneys filter the systemic blood supply by two mechanisms: passive filtration through the glomerulus and active tubular secretion. Approximately 20% of renal plasma flow is filtered and 80% is secreted. The glomerulus primarily filters larger compounds out of the urine, although some larger proteins are excreted into the urine by active secretion from the tubules.

Radiopharmaceuticals

While many radiopharmaceuticals have been used for renal imaging, the most common in clinical practice include technetium-99m (Tc-99m) mercaptoacetyltriglycerine (MAG3), Tc-99m dimercaptosuccinic acid (DMSA), Tc-99m diethylenetriaminepentaacetic acid (DTPA), and Tc-99m sulfur colloid. Tc-99m MAG3 is the most frequently used renal radiopharmaceutical in the United States (approximately 70% of cases) and is almost completely cleared by tubular secretion.[1] Tc-99m MAG3 clearance correlates well with effective renal plasma flow and can be used as an independent measure of renal function. Tc-99m DMSA is the radiopharmaceutical of choice for renal cortical imaging, since it binds to sulfhydryl groups on the proximal convoluted tubule, allowing for minimal cortical transit. Tc-99m DTPA is a heavy metal chelator that is cleared by glomerular filtration. Tc-99 DTPA is used primarily for glomerular filtration rate (GFR) analysis, but may also be used in evaluation for renovascular hypertension.[2] Tc-99m sulfur colloid is the preferred radiopharmaceutical in the evaluation for vesicoureteral reflux.

Dynamic Renography

Dynamic renography can be used to assess overall and differential renal function. In terms of patient preparation, patients should be instructed to drink plenty of water prior to the examination, as dehydration can affect the results.[2] It is also recommended that patients void immediately following the procedure to reduce radiation exposure to the pelvic structures.[2]

After Tc-99m MAG3 is administered intravenously, posterior dynamic images are obtained for a total of approximately 30 minutes. Images are acquired every 1 to 5 seconds for the first minute to assess renal perfusion. One-minute images are then obtained for the remainder of the exam to evaluate cortical uptake and transit, as well as excretion.

Regions of interest (ROIs) are placed over each kidney and the aorta, with additional background ROIs inferior to each kidney, allowing for creation of time-activity curves (TACs) (**Figure 1**). The TACs allow for quantitative analysis of renal perfusion and function with regard to radiopharmaceutical uptake and excretion. Separate TACs can be created using ROIs encompassing the entire kidney, just the renal cortex, or the collecting system. Adjusting the ROIs may be necessary for accurate interpretation, especially in cases with collecting system retention (**Figure 2**).[1]

Renal uptake should occur around the same time as visualization of the aortic bifurcation on the initial dynamic images, with peak renal activity equal to or exceeding the aorta. The kidneys should also demonstrate symmetric activity/flow.[4] A delay in visualization of the kidneys or decreased peak activity suggests abnormal perfusion. If both the renal and aortic flow curves demonstrate a slow rather than rapid rise, it

FIGURE 1. *Standard ROIs for dynamic renography. Representative image from dynamic renography showing ROIs drawn around the left kidney (white), right kidney (blue), aorta (red), left renal background (yellow), right renal background (light green) and bladder (pink). These ROIs allow for the creation of background-corrected time-activity curves for quantitative analysis of renal perfusion and function.*

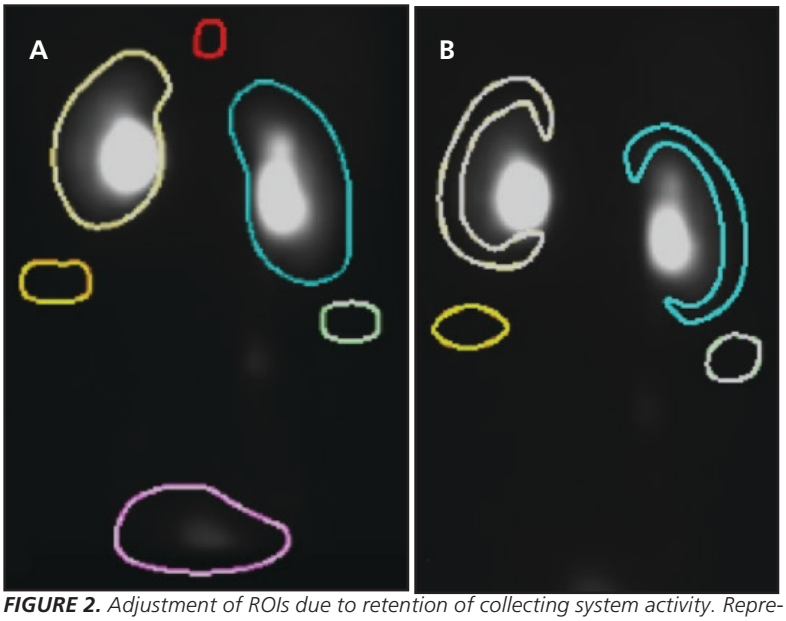

FIGURE 2. *Adjustment of ROIs due to retention of collecting system activity. Representative image from dynamic renography showing whole kidney ROIs (A) and cortical ROIs (B). While most quantitative data can be derived from the whole kidney ROIs, the cortical ROIs may be necessary to accurately evaluate cortical residual if there is retained collecting system activity at 20 minutes.*

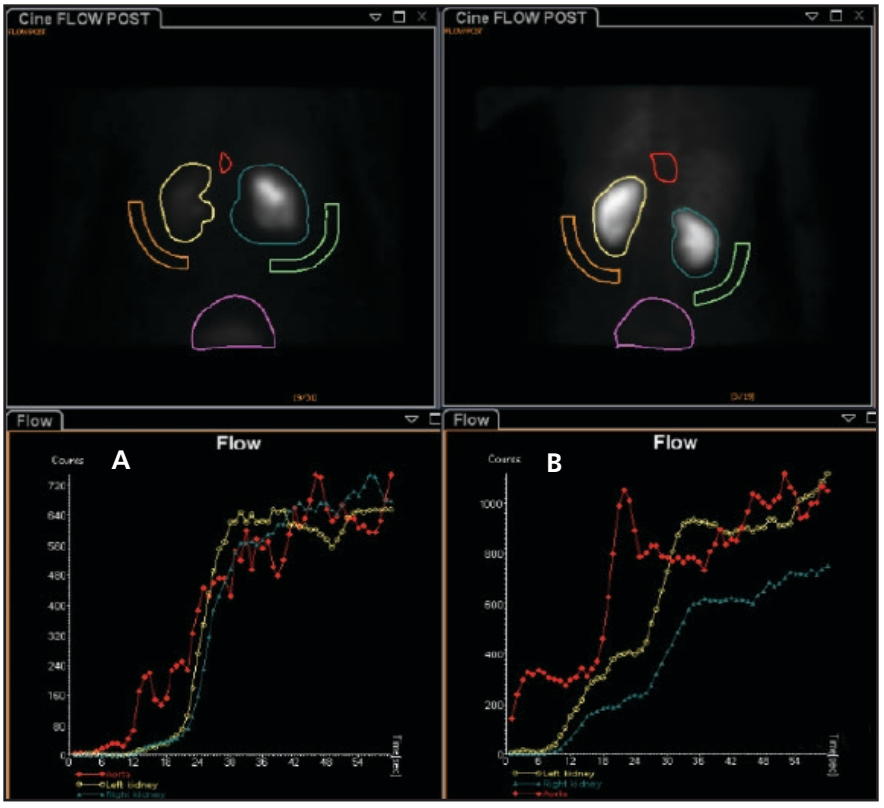

FIGURE 3. *Flow curves with adequate and poor injection bolus. Normal (A) and abnormal (B) renal flow time activity curves generated from initial 1-second dynamic images for 60 seconds after injection of Tc-99m MAG3. Notice the slow rise to peak in the abnormal curve (B) for the aorta and both kidneys compared to relative rapid rise with an adequate bolus (A), suggesting a poor bolus (bad injection technique or extravasation).*

is likely due to a poor injection bolus (**Figure 3**).[5]

Peak cortical activity should occur within 3 to 5 minutes, with half of the peak activity (T1/2) cleared from the kidney at 8 to 12 minutes. Less than 30% of peak activity should remain within the renal cortex at 20 minutes (**Figure 4**).[2] A delay in cortical time to peak, prolonged cortical transit, or increased 20-minute cortical residual are nonspecific indicators of nephron dysfunction from acute or chronic renal disease (**Figure 5**).

Excretion is evaluated by determining the washout half-time (T1/2), which refers to the time from either peak activity to one-half peak activity, or with diuretic renography (discussed below) from the activity at the time of furosemide injection to one-half of that activity. T1/2 is considered normal if it is < 10 minutes.[6]

Differential function is usually calculated using the counts obtained between 2 and 3 minutes from the whole kidney ROIs. This should prevent inclusion of any significant collecting system activity. Differential function should be approximately equal between the kidneys

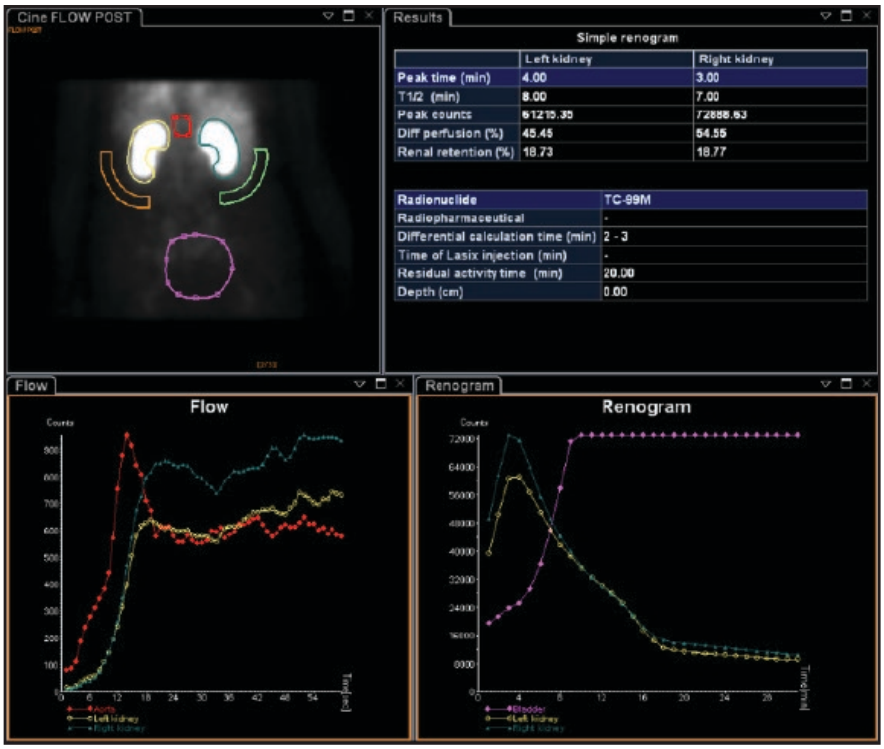

FIGURE 4. *Summary image from a normal dynamic renogram. Both kidneys have a time to peak of < 5 minutes, a T1/2 (time from peak to half peak) of < 10 minutes, 20-minute renal retention < 30%, and differential function between 45% and 55%.*

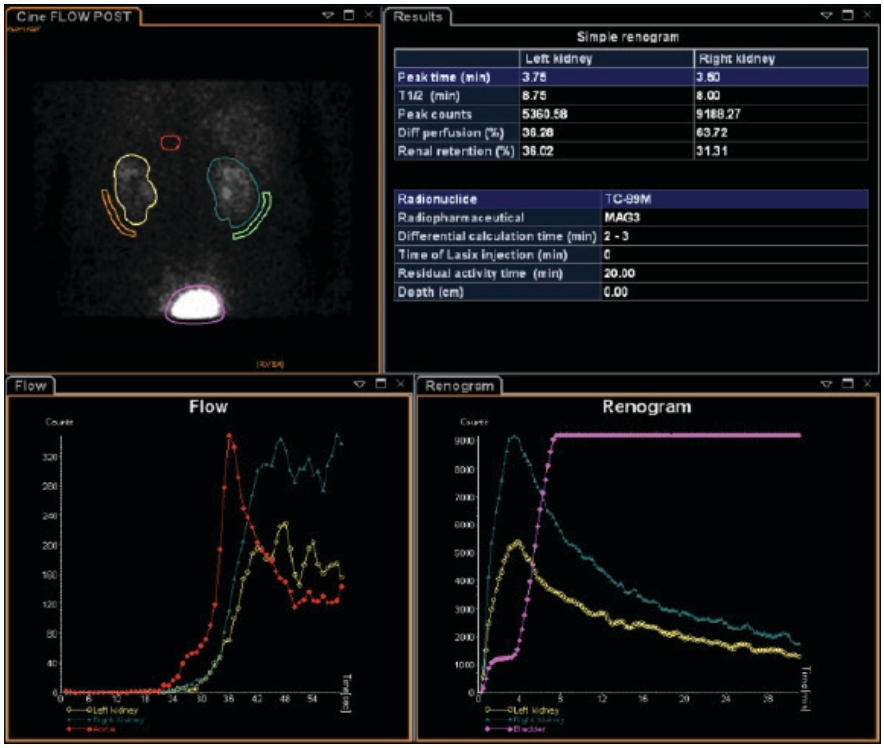

FIGURE 5. *Dynamic renography showing renal dysfunction. Dynamic renography showing decreased left kidney perfusion/function, approximately 36% on the left compared to 64% on the right, along with bilateral mildly increased 20-minute renal retention suggesting nephron dysfunction. This study was performed without furosemide; the time of furosemide was entered as 0 minutes to allow for quantitative analysis.*

with an acceptable range of a few percentage points to allow for differences in overlying attenuation. We use 45% to 55% as normal at our institution. No significant difference in differential function has been demonstrated between men and women.[7]

Diuretic Renography

While anatomic imaging can demonstrate dilation of the genitourinary collecting system, it is less reliable in delineating between obstructive and nonobstructive causes in the absence of a visualized source of obstruction. A patulous system with decreased peristalsis can result in dilation of the renal collecting system in the absence of a mechanical obstruction in a variety of clinical settings, to include vesicoureteral reflux (VUR), megaureter, and prior mechanical obstruction or infection.[4] Diuretic renography can be helpful in these clinical scenarios.

Diuretic renography involves the addition of intravenous (IV) furosemide, a loop diuretic, to the dynamic renography study. It is important to first verify whether the patient is allergic to sulfa medications, as there is some degree of cross-reactivity with furosemide.[8] Diuretic renography may be performed in one of three ways based on the timing of furosemide injection. The first option is to administer roughly 40 mg of IV furosemide (with dose adjusted for renal function and weight) at the same time as the radiopharmaceutical (MAG3) using the same imaging parameters discussed above under dynamic renography. This is referred to as the F+0 protocol. The second option is to perform the dynamic renography protocol as above and assess the need for furosemide administration at the 20-minute mark. If the examination is normal up to that point, then the study is complete without the need for diuretic administration. If the study is abnormal based on the parameters above, then the diuretic is administered at this point with continued imaging over the next 30 minutes. This is referred to as the F+20 protocol. The third option involves injecting the diuretic 15 minutes prior to

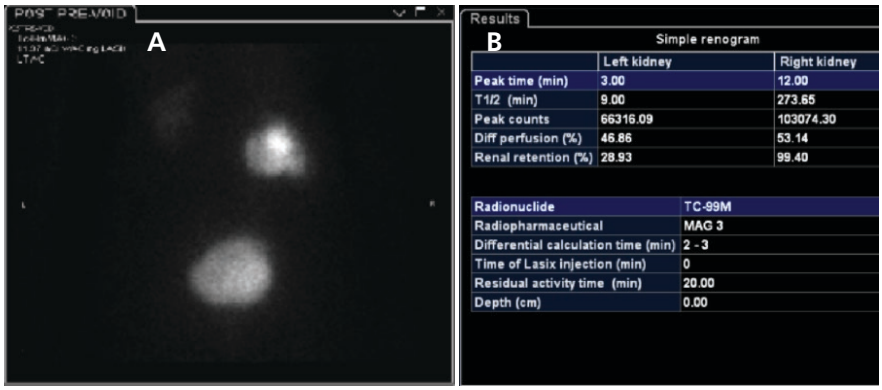

FIGURE 6. *Diuretic renography demonstrating a mechanical obstruction. Composite image from diuretic renography performed with furosemide administered at time 0 (A) demonstrates retention in the proximal right renal collecting system. Quantitative analysis of the time activity curves from this study (B) shows a markedly delayed T1/2 on the right of approximately 274 minutes, consistent with severe right ureteropelvic junction obstruction.*

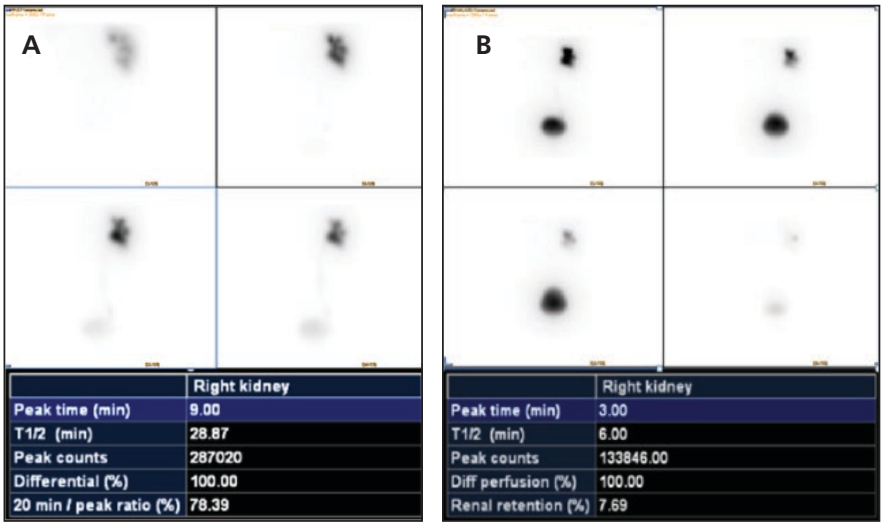

FIGURE 7. *Diuretic renography demonstrating a functional, nonmechanical obstruction. Five-minute compressed images pre- (A) and post- (B) furosemide administration with associated quantitative analyses, demonstrating right renal collecting system retention that washes out normally after diuretic administration. The abnormally elevated T1/2 washout prior to furosemide administration (approximately 29 minutes, A) normalizes after diuretic administration (6 minutes, B). The left kidney is congenitally absent.*

radiopharmaceutical administration and then completing dynamic renography as described previously. Referred to as the F-15 protocol, this decreases the likelihood of a false positive exam by delaying imaging until after the peak effect of furosemide is reached.[9]

If collecting system dilation is due to a mechanical obstruction (eg, stone, stricture or mass), delayed washout of collecting system activity will be seen even after the administration of IV furosemide (**Figure 6**). If the dilation is not the result of an underlying mechanical obstruction, the increased urine production after diuretic administration will increase hydrostatic pressure enough to wash out the patulous system and T1/2 will normalize on dynamic renography (**Figure 7**).[10] This process requires functioning renal tissue for the diuretic effect and can be negated by dehydration. T1/2 washout is considered normal if it occurs < 10 minutes after diuretic administration and abnormal if it is > 20 minutes.[6] The 10 to 20 minute timeframe is less specific. At our institution, values of 10 to 15 minutes are generally deemed likely not obstructed, and values of 15 to 20 minutes are deemed likely obstructed.

Washout parameters from dynamic renography for patients with a dilated but not obstructed system will be normal if the diuretic is administered at the same time as (F+0 protocol), or prior to (F-15 protocol) administration of the radiopharmaceutical (**Figure 8**).

Renal Cortical Imaging

Renal cortical imaging with Tc-99m DMSA is useful in evaluating focal cortical abnormalities, such as pyelonephritis, space-occupying lesions, columns of Bertin (functional pseudotumors), and parenchymal scarring.[11]

Pyelonephritis refers to an infection involving the kidneys and has a variety of imaging appearances to include single or multiple cortical defects, and localized or diffuse decreased activity in one or both kidneys.[12] Scintigraphy is sensitive for pyelonephritis and is especially useful in excluding pyelonephritis (with a normal study) in pediatric patients who often present with more challenging clinical symptoms. The primary limitation is the lack of specificity for an underlying infectious process.

For the imaging protocol, a weight-based dose of Tc-99m DMSA is administered, typically with a minimum of 500 μCi. Posterior and oblique images of the kidneys are obtained. Single-photon emission computed tomography (SPECT) images are also frequently obtained and often helpful.[13] Normal kidneys will show homogenous uptake throughout the renal cortex; minimal heterogeneity secondary to renal cortical columns may be seen if a high-resolution collimator is used. In the acute phase of pyelonephritis, the defects are likely attributable to edema and relative ischemia of the renal parenchyma.[14] These defects may resolve over time. However, if there is permanent scarring, cortical defects can develop with associated renal volume loss (**Figure 9**).[15]

Tc-99m DMSA scanning can also be used to assess renal masses to differentiate functional renal parenchyma from a space-occupying lesion. Space-occupying lesions, such as cysts, neoplasms, hematomas, abscesses, infarcts, and

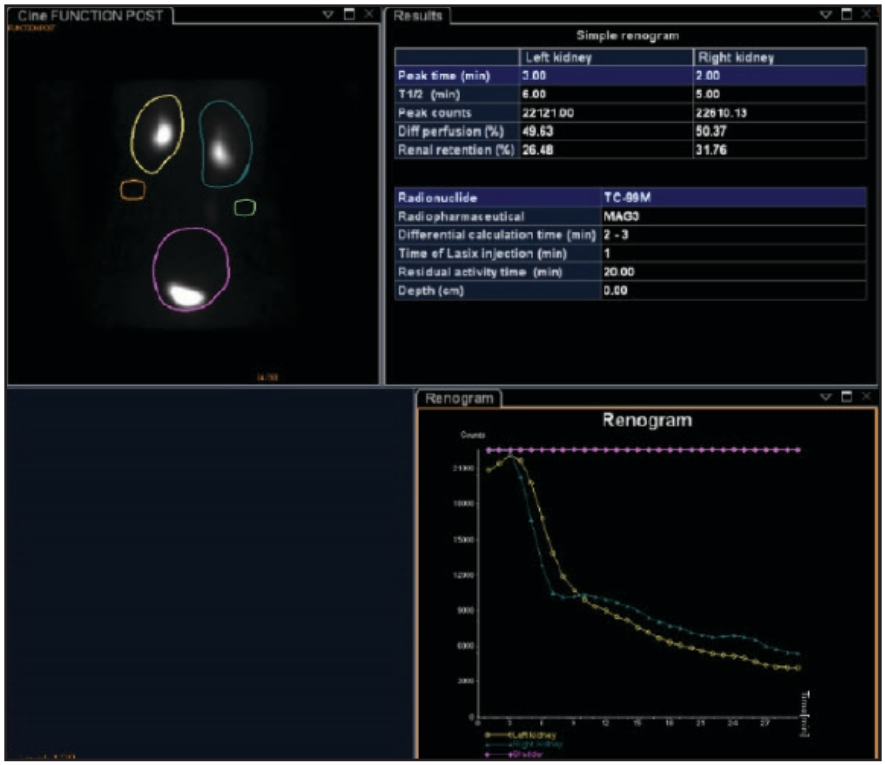

FIGURE 8. *Diuretic renography with furosemide and Tc-99m MAG3 administered at the same time (F+0 protocol). Postfurosemide renogram in a patient with right-sided hydronephrosis noted on renal ultrasound demonstrating normal washout of radiotracer with a T1/2 of 5 minutes on the right, excluding mechanical obstruction.*

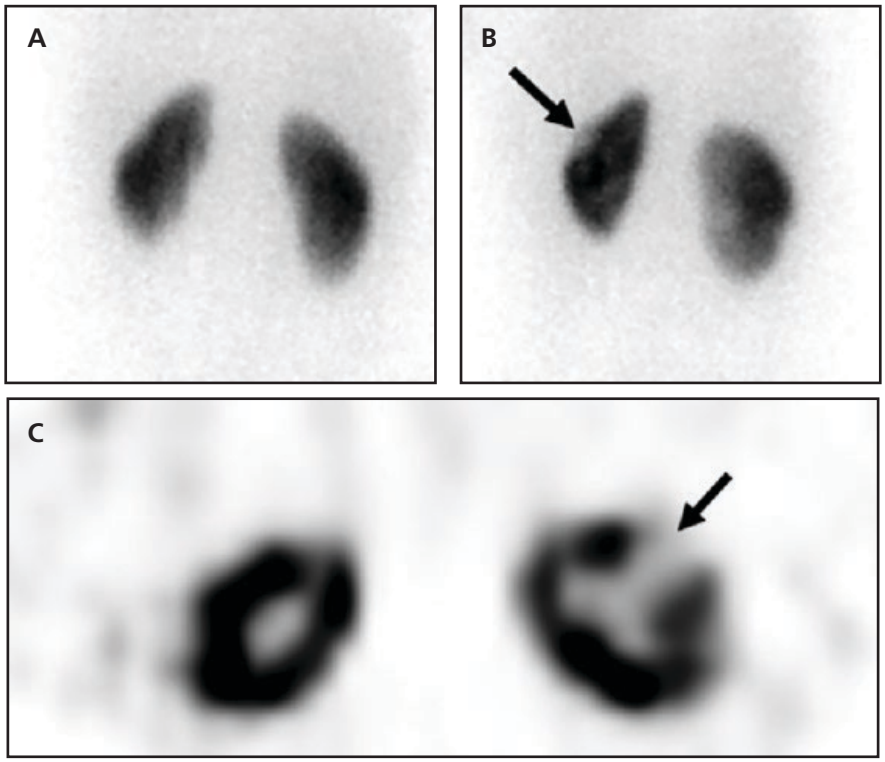

FIGURE 9. *Scarring on renal cortical imaging. Posterior, LPO, and transverse SPECT image from a Tc-99m DMSA renal scan demonstrates a wedge-shaped cortical defect in the mid to upper left kidney. This correlated with a region of cortical scarring on CT.*

regions of scarring, will have focal decreased activity when compared to the adjacent renal parenchyma.[11] Although a focal region of decreased activity is not specific to a particular pathologic process, it excludes normal renal tissue that may mimic a mass on other imaging modalities. Examples of normal variant and functional renal tissue that may mimic a mass include prominent columns of Bertin, fetal lobulation, and dromedary humps, all of which demonstrate normal radiopharmaceutical activity.[4]

Angiotensin-converting Enzyme Inhibitor (ACEI) Renography

Renal artery stenosis (RAS), usually due to atherosclerosis or fibromuscular dysplasia, is a relatively uncommon but important cause of hypertension. The associated hypertension is a result of the normal physiologic mechanisms designed to maintain glomerular filtration pressure. When there is decreased renal perfusion pressure secondary to RAS, renin is released by the juxtaglomerular apparatus (JGA). Renin is converted to angiotensin I (ATI) by angiotensinogen in the liver, which, in turn, is converted by ACE in the lungs to angiotensin II (ATII). ATII is vasoactive and results in vasoconstriction of the efferent arteriole, thus increasing pressure across the glomerulus.

Dynamic renography utilizing ACEI administration can help diagnose renovascular hypertension in at-risk patients, as there are no discriminatory clinical findings.[16] The ACEI works by preventing the conversion of ATI to ATII in the lungs, thus preventing the compensatory renal vasoconstriction of the efferent arteriole. At-risk patients include those who initially present with hypertension before 30 or after 55 years of age; have severe or accelerated hypertension refractory to medical management; experience new difficulty with medical management; have evidence of occlusive vascular disease on other imaging modalities; have decreased renal function with recent hypertension; and/or exhibit abdominal pain or bruits auscultated over

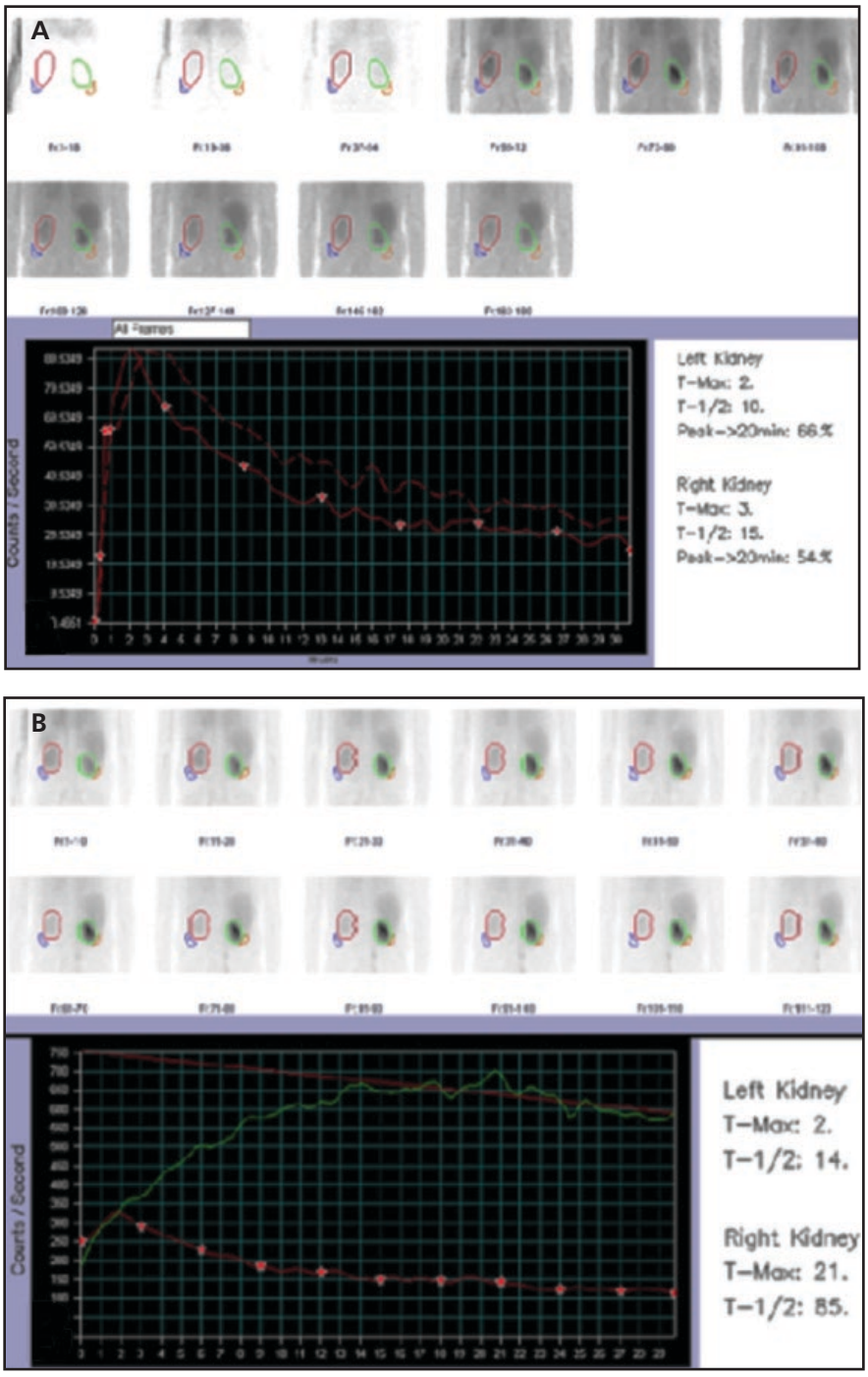

FIGURE 10. *Renal artery stenosis on ACEI renography. Baseline (A) and postenalapril (B) Tc-99m MAG3 dynamic renography shows marked increased cortical retention in the right kidney after the administration of the ACEI (green line, B). This is high probability for renovascular hypertension. (Case courtesy of Dr. Joseph Fotos, Penn State Hershey Medical Center).*

the flanks.[17] The primary goal of ACEI renography is to identify patients who would benefit from correction of the underlying renal artery stenosis.

Prior to ACEI renography, patients should discontinue captopril 48 hours, and lisinorpil or enalapril 1 week, prior to the exam. They are also encouraged to be well-hydrated and to fast prior to the exam to improve the absorption of oral captopril administered as part of the study.[18] Calcium channel blockers should also be discontinued as they have been shown to result in a false positive exam with bilateral decreased renal function.[19]

Protocols for ACEI renography generally involve a one- or two-day study. With a two-day protocol, an ACEI study is initially performed. If the study is normal, no further imaging is necessary. If abnormal, the patient returns on day two for a baseline study. The one-day protocol involves obtaining a baseline study with a low dose of radiopharmaceutical several hours prior to the ACEI study. Furosemide may be administered to clear the renal collection system.[20] An ACEI study is performed approximately one hour following the oral administration of 25-50 mg of captopril or 15 minutes after 0.04mg/kg of IV enalapril.[17] Ten mCi of Tc-99m MAG3 or DTPA is administered intravenously and renal scintigraphy is performed.

An ACEI study is abnormal when the renogram is asymmetric or becomes more abnormal when compared to the baseline renogram due to a drop in GFR caused by ACEI administration. When DTPA is used, a patient with renovascular hypertension will show diminished uptake and excretion on the ACEI study.[18] When MAG3 is administered, an abnormal study will show increased cortical retention as tubular secretion is not affected, but the drop in GFR prevents washout of the tubular activity (**Figure 10**).[18]

Diagnostic criteria for RAS on a Tc-99m MAG 3 study include < 40% renal uptake at 2 to 3 minutes, retained cortical activity at 20 minutes that is > 20% asymmetric compared to the contralateral normal side or increased ≥ 15% from baseline (ipsilateral), or a delay in the time to peak activity > 2 minutes compared to baseline.[21] Quantitative abnormalities should be confirmed on the qualitative data. Maintaining hydration throughout the exam is paramount, as both hypotension and dehydration can affect the renograms.[5]

In terms of reporting, a normal study or an abnormal baseline study that improves with ACEI is considered low

FIGURE 11. *Vesicoureteral reflux on radionuclide cystography. Image from a Tc-99m sulfur colloid VCUG demonstrating activity within the bladder and bilateral reflux into the collecting system up to the level of the renal collecting system (moderate VUR).*

probability (< 10%) for renovascular hypertension. If the baseline study is abnormal but is unchanged with ACEI, then it is considered intermediate probability for renovascular hypertension. High probability (> 90%) is reported when detrimental changes from baseline are seen after ACEI administration.[21]

Radionuclide Cystography (RNC)

While vesicoureteral reflux (VUR) is typically evaluated with a fluoroscopic voiding cystourethrogram (VCUG) initially, it is often followed up with radionuclide cystography (RNC). RNC may also be used in evaluating siblings of patients diagnosed with VUR.[20] While RNC does not present the same level of detailed anatomic evaluation of VUR and cannot diagnose posterior urethral valves in a boy, it does prove a useful tool to confirm persistence or resolution of VUR. The benefits of RNC over VCUG include likely decreased radiation dose and increased sensitivity for small volume and intermittent reflux.[22]

RNC is performed by injecting a mixture of 0.5 to 1 mCi of Tc-99m sulfur colloid and saline through a bladder catheter, injecting enough volume to adequately fill the urinary bladder. Dynamic posterior images are obtained through at least one filling and voiding cycle. In a normal study, no radiopharmaceutical is visualized outside of the bladder. If reflux does occur, it may be seen during initial filling of the bladder, as the patient voids, or even on postvoid imaging. While reflux evaluated by fluoroscopic VCUG is categorized into one of five types based on varying severity, it is characterized as one of three variants (minimal, moderate, or severe) with radionuclide imaging. Minimal reflux is defined as radiopharmaceutical contained within the ureter(s), moderate if counts reach the pelvicalyceal system, and severe if the involved pelvicalyceal system appears dilated or the ureter is tortuous (**Figure 11**).[4]

The postvoid residual bladder volume can also be calculated by using the bladder counts before and after voiding. This quantitative assessment may be inaccurate in the setting of significant reflux, as the activity in the collecting system re-enters the bladder postvoid.[23]

Summary

Scintigraphy plays an important role in the evaluation of a variety of genitourinary pathologies. Its ability to assess renal function complements other cross-sectional modalities that rely more on anatomic assessment. Having a fundamental knowledge of the radiopharmaceuticals, clinical applications, and common pathologies is essential for those involved with interpretation of genitourinary nuclear medicine studies.

References

1. Taylor AT. Radionuclides in nephrourology, part 1: radiopharmaceuticals, quality control and quantitative indices. J Nucl Med 2014;55(4)608-615.
2. Taylor A, Nally JV. Clinical applications of renal scintigraphy. Am J Roentgenol 1995;164(1):31-41.
3. Esteves FP, Taylor A, Manatunga A, et al. 99mTc-MAG3 renography: normal values for MAG3 clearance and curve parameters, excretory parameters, and residual urine volume. Am J Roentgenol 2006;187(6):W610-W617.
4. Mettler FA, Guibeteau MJ. Genitourinary system and adrenal glands. In: Essentials of Nuclear Medicine Imaging. 5th Ed. Philadelphia, PA: Saunders Elsevier; 2006:293-324.
5. Keramida G, James JM, Prescott MC, Peters AM. Pitfalls and limitations of radionuclide renal imaging in adults. Semin Nucl Med 2015;45(5):428-439.
6. Karam M, Feustel PJ, Goldfarb CR, et al. Diuretic renogram clearance half-times in the diagnosis of obstructive uropathy: effect of age and previous surgery. Nucl Med Commun 2003;24(7):797-807.
7. Taylor AT, Garcia EV. Computer assisted diagnosis in renal nuclear medicine: rationale, methodology and interpretative criteria for diuretic renography. Semin Nucl Med 2014;44(2):146-158.
8. Slatore CG, Tilles SA. Sulfonamide hypersensitivity. Immunol Allergy Clin N Am 2004;24:477-490.
9. Türkölmez S, Atasever T, Türkölmez K, et al. Comparison of three different diuretic renal scintigraphy protocols in patients with dilated upper urinary tracts. Clin Nucl Med 2004:29(3);154-160.
10. Livnat U, Mellnick V, Menias C, et al. Nuclear medicine in the acute clinical setting: indications, imaging findings, and potential pitfalls. Radiographics 2013:33;375-396.
11. Blaufox MD. Procedures of choice in renal nuclear medicine. J Nucl Med 1991;32(6):1301-1309.
12. Lavocat MP, Granjon D, Allard D, et al. Imaging of pyelonephritis. Pediatr Radiol 1997;27:159-165.
13. Rossleigh MA. Renal cortical scintigraphy and diuresis renography in infants and children. J Nucl Med 2001;42(1):91-95.
14. Björgvinsson E, Majd M, Eggli KD. Diagnosis of acute pyelonephritis in children: comparison of sonography and Tc-99m DMSA scintigraphy. Am J Roentgenol 1990;157(1):539-543.
15. Agras K, Ortapamuk H, Naldöken S, et al. Resolution of cortical lesions on serial renal scans in children with acute pyelonephritis. Pediatr Radiol 2007;37(2):153-158.
16. Soulez G, Oliva VL, Turpin S, et al. Imaging of renovascular hypertension: respective values of renal scintigraphy, renal doppler US, and MR angiography. Radiographics 2000;20(5):1355-1368.
17. Taylor AT. Radionuclide in nephrourology, part 2: pitfalls and diagnostic applications. J Nucl Med 2014;55(5):786-798.
18. Taylor A, Nally J, Aurell M, et al. Consensus report on ACE inhibitor renography for detecting renovascular hypertension. J Nucl Med 1996;37:1876-1882.
19. Claveau-Tremblay R, Turpin S, De Braekeleer M, et al. False-positive captopril renography in patients taking calcium antagonists. J Nucl Med 1998;39(9):1621-1626.
20. Boubaker A, Prior JO, Meuwly JY, et al. Radionuclide investigations of the urinary tract in the era of multimodality imaging. J Nucl Med 2006;47:1819-1836.
21. Taylor AT Jr, Blaufox MD, Dubovsky EV, et al. Society of Nuclear Medicine procedure guideline for diagnosis of renovascular hypertension version 3.0. Society of Nuclear Medicine 2003;Aug:97-104.
22. Piepsz A, Ham HR. Pediatric applications of renal nuclear medicine. Semin Nucl Med 2006;36:16-35.
23. ACR–SPR–SNM Practice guideline for the performance of adult and pediatric radionuclide cystography, Revised 2010 (Resolution 39). http://snmmi.files.cms-plus.com/docs/Radionuclide_Cystography_1382732076756_9.pdf. Accessed April 29, 2016.

Disclaimer: *The views expressed in this article are those of the author and do not necessarily reflect the official policy or position of the Department of the Air Force, Department of Defense, or the U.S. Government.*

Hypermetabolic Appendiceal Activity on PET-CT

Joseph M. Yetto, Jr., M.D., Frederic C. Jewett, III, D.O., Mickaila J. Johnston, M.D.

Department of Radiology, Naval Medical Center San Diego, San Diego, CA

Case Presentation

We present a 9-year-old girl with a history significant for 8 months of left wrist pain, which ultimately led to the diagnosis of stage IV diffuse large B-cell lymphoma (DLBCL). Initial fluorine 18 fluorodeoxyglucose (FDG) positron emission tomography-computed tomography (PET-CT) imaging revealed hypermetabolic activity in the left wrist, as well as in right inguinal and left axillary lymphadenopathy. The patient underwent chemotherapy and completed the last cycle of R-CHOP (chemotherapy regimen consisting of rituximab, cyclophosphamide, hydroxydaunorubicin, vincristine [Oncovin], and prednisone). A follow-up FDG PET-CT to determine treatment response revealed complete response in the noted hypermetabolic areas. However, there was a new area of focal hypermetabolic activity centered in the appendix (**Figure 1**).

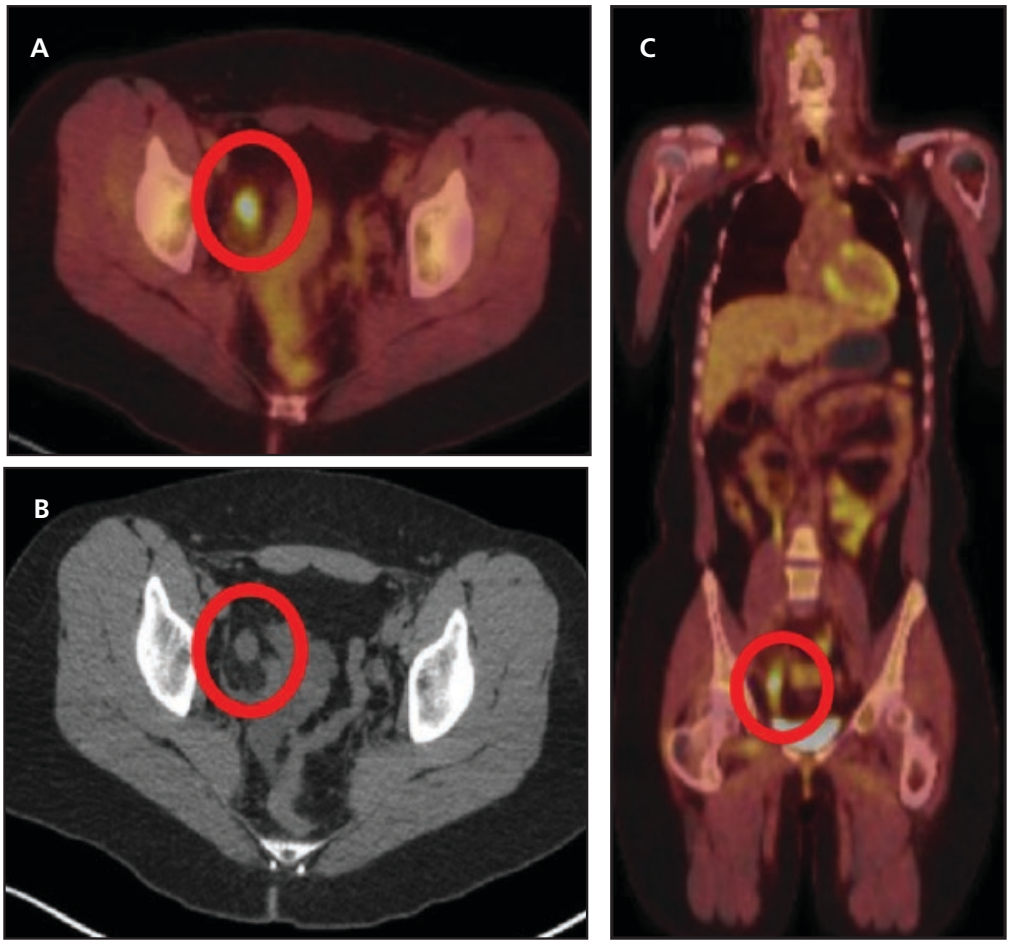

FIGURE 1. *Axial and coronal fused PET-CT images (A, C) show a focal region of hypermetabolic activity within the right lower quadrant (encircled). Corresponding unenhanced axial CT image (B) reveals a dilated appendix with no luminal air and mild adjacent fat stranding (encircled).*

Key Imaging Finding

Hypermetabolic appendix

Differential Diagnoses

Infectious/inflammatory process
Primary neoplasm
Metastatic disease

Discussion

FDG PET-CT is commonly used in evaluating neoplastic processes due to the high lesion-to-background contrast from the increased metabolic activity of tumor cells.[1,2] FDG PET-CT is in most cases effective for evaluating the primary lesion as well as determining the extent/stage of disease and monitoring therapy. However, FDG is not tumor-specific as many benign and physiologic processes also demonstrate FDG avidity.[2] FDG PET-CT is, therefore, capable of detecting a wide range of gastrointestinal tumors and inflammatory conditions. However, the interpreter must remain cognizant that an area of avidity may not reflect pathology related to the primary indication.[1]

Primary appendiceal neoplasms are rare. They generally have no characteristic signs or symptoms, but may result in acute appendicitis secondary to occlusion from mass effect.[3]

Infectious/Inflammatory Process

Appendicitis refers to inflammation of the vermiform appendix. Patients often present with fever, nausea, vomiting, anorexia, leukocytosis, and initially periumbilical pain, which eventually localizes to the right lower quadrant as the appendix becomes increasingly inflamed and irritates the adjacent abdominal wall. Ultrasound and CT are the two most common imaging modalities for suspected acute appendicitis, demonstrating a dilated, fluid-filled appendix with surrounding inflammatory changes. With ultrasound, lack of ionizing radiation makes it the preferred initial method for appendicitis evaluation in children and pregnant patients.

While FDG PET-CT should not be used for evaluation of suspected acute appendicitis, FDG PET-CT may occasionally suggest the diagnosis when it is an incidental finding or is unsuspected, such as in patients with a fever of unknown origin. On FDG PET-CT, acute appendicitis presents as focal hypermetabolic activity overlying an enlarged and dilated appendix with periappendiceal fat stranding.[4] Typhlitis, a life-threating necrotizing enterocolitis involving the ileocecal region predominantly seen in neutropenic patients, may demonstrate similar increased FDG avidity in the region of the appendix with involvement of the adjacent bowel.

Inflammatory bowel disease, most commonly Crohn's disease, may also result in active inflammation of the appendix that can be detected on FDG PET-CT. In general, FDG PET-CT is a sensitive, noninvasive method for detecting and monitoring active bowel inflammation. However, as mentioned, FDG avidity is not specific; therefore, the clinical history will drive interpretation of areas of hypermetabolic intra-abdominal activity.[5]

Primary Neoplasm

Mucinous cystadenocarcinoma of the appendix is one of the more common noncarcinoid malignant neoplasms of the appendix. It is a high-grade tumor that can metastasize to the regional lymph nodes, liver and lungs. Mucinous neoplasms can rupture, resulting in gelatinous material accumulating within the peritoneal space, or pseudomyxoma peritonei.[6] High-grade neoplasms preferentially take up FDG and, thus, are hypermetabolic on FDG PET-CT.[7] The most common clinical presentation of this tumor is superimposed acute appendicitis.

The gastrointestinal tract is the most common site for extranodal lymphoma, although primary lymphoma of the appendix is rare. Lymphoma can present clinically similar to acute appendicitis, but more commonly demonstrates an insidious onset. Primary lymphoma of the appendix is almost always non-Hodgkin lymphoma, which demonstrates variable FDG avidity.[8]

Carcinoid tumor, a neuroendocrine neoplasm and the most common tumor of the appendix, is usually incidentally detected on appendectomy.[9] These are typically small (< 1 cm) tumors, limiting their detection on anatomic imaging.[9] Many have nodal and distant metastases, classically hypervascular on contrast-enhanced CT, at the time of diagnosis. FDG PET-CT is often limited, as many carcinoid tumors are low-grade with low glycolytic rates, but FDG avidity often indicates a worse prognosis.[9]

Metastatic Disease

The most common metastases to the appendix are from neoplasms of the breast, colon, and female reproductive organs.[10] Metastases to the appendix can present as acute appendicitis due to luminal obstruction. Metastatic disease demonstrates similar FDG uptake variability based on the type of primary tumor and the degree of differentiation of the metastases.

Diagnosis

Acute suppurative transmural appendicitis

Patient Follow-up

FDG PET-CT findings were highly suspicious for acute appendicitis even in this patient with known stage IV DLBCL. At the time of interpretation, the ordering provider was contacted and informed of the findings. The patient was then sent to the local emergency department where she was found to have an acute abdomen on physical exam and subsequently underwent an uncomplicated laparoscopic appendectomy, which revealed acute suppurative transmural appendicitis on pathology examination.

Summary

FDG PET-CT is commonly used in the evaluation of neoplastic processes;

however, FDG avidity is not tumor-specific, as a myriad of infectious and inflammatory processes may show increased metabolic activity as well. This case of acute appendicitis illustrates that the interpreter of PET-CT images must consider that FDG activity may reflect pathology unrelated to the primary indication for the exam.

References

1. Kamel EM, Thumshirn M, Truninger K, et al. Significance of incidental 18F-FDG accumulations in the gastrointestinal tract in PET/CT: correlation with endoscopic and histopathologic results. J Nucl Med 2004;45(11):1804-1810.
2. Israel O, Yefremov N, Bar-Shalom R, et al. PET/CT detection of unexpected gastrointestinal foci of 18F-FDG uptake: incidence, localization patterns, and clinical significance. J Nucl Med 2005;46(5):758-762.
3. Park HL, Yoo IeR, Choi EK, et al. Acute appendicitis secondary to metastatic small cell lung cancer incidentally found on F-18 FDG PET/CT. Clin Nucl Med 2012;37(1):e19-21.
4. Moghadam-Kia S, Nawaz A, Newberg A, et al. Utility of 18F-FDG-PET/CT imaging in the diagnosis of appendicitis. Hell J Nucl Med 2009;12(3): 281-282.
5. Perlman SB, Hall BS, Reichelderfer M. PET/CT imaging of inflammatory bowel disease. Semin Nucl Med 2013;43(6):420-426.
6. Pickhardt PF, Levy AD, Rohrmann CA, et al. Primary neoplasms of the appendix: radiologic spectrum of disease with pathologic correlation. RadioGraphics 2003;23:645-662.
7. Passot G, Glehen O, Pellet O, et al. Pseudomyxoma peritonei: role of 18F-FDG PET in preoperative evaluation of pathological grade and potential for complete cytoreduction. Eur J Surg Oncol 2010;36(3):315-323.
8. Tsukamoto N, Kojima M, Hasegawa M, et al. The usefulness of (18)F-fluorodeoxyglucose positron emission tomography ((18)F-FDG-PET) and a comparison of (18)F-FDG-PET with (67)gallium scintigraphy in the evaluation of lymphoma: relation to histologic subtypes based on the World Health Organization classification. Cancer 2007;110(3):652-659.
9. Ganeshan D, Bhosale P, Yang T, Kundra V. Imaging features of carcinoid tumors of the gastrointestinal tract. AJR Am J Roentgenol 2013;201(4):773-786.
10. Kim HC, Yang DM, Jin W, Kim GY, Choi SI. Metastasis to the appendix from a hepatocellular carcinoma manifesting as acute appendicitis: CT findings. Br J Radiol 2008;81(967):e194-196.

Disclaimer: *The views expressed in this article are those of the author and do not necessarily reflect the official policy or position of the Department of the Navy, Department of Defense, or the U.S. Government.*

Radiographically Benign-Appearing Lesion in Child with Uptake on Bone Scan

Victoria A. Campbell, M.D., Michael D. Starsiak, M.D., Mickaila J. Johnston, M.D.

Department of Radiology, Naval Medical Center San Diego, San Diego, CA

Case Presentation

A previously healthy 8-year-old boy presented to the emergency department after falling from monkey bars. He was unable to bear weight and was found to have a right proximal femur fracture extending through a mixed sclerotic and lytic lesion. The lesion was eccentric and demonstrated a thin sclerotic rim with no periosteal reaction (**Figure 1A**). Additional similar lesions were throughout the right femur. Tc99m MDP bone scintigraphy revealed additional lesions in the tibia and pelvis (**Figure 1B**).

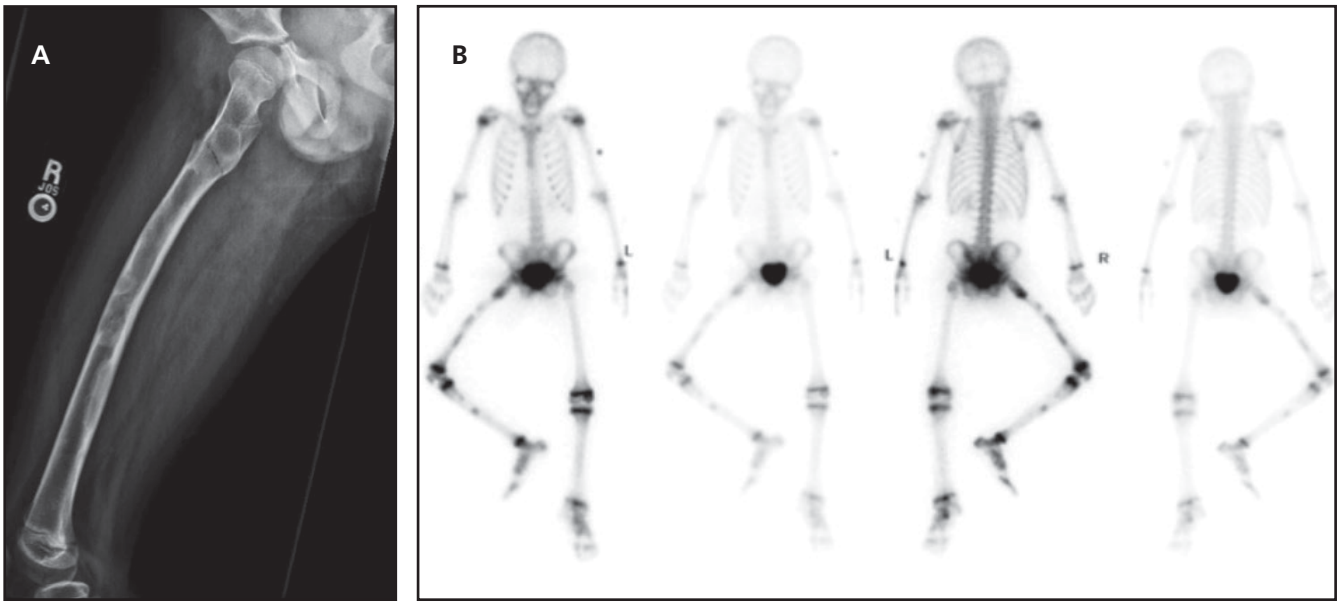

FIGURE 1. *Right femur radiograph (A) demonstrates a pathologic facture through a nonaggressive-appearing mixed lytic and sclerotic lesion of the proximal femur. Similar appearing lesions are noted throughout the mid to distal femur. Tc99m bone scan (B) demonstrates multiple foci of increased radiotracer uptake within the right lower extremity, consistent with a polyostotic process.*

Key Imaging Finding

Radiographically benign-appearing lesion in a pediatric patient with uptake on bone scan

Differential Diagnosis

Fibrous dysplasia
Nonossifying fibroma
Langerhans cell histiocytosis
Osteomyelitis

Discussion

The radiographic appearance of a lesion with a sharp border and narrow zone of transition is extremely reassuring for benignity in the pediatric population. Primary considerations for a nonaggressive-appearing bone lesion in this age group include fibrous dysplasia, nonossifying fibroma (NOF), Langerhans cell histiocytosis (LCH) and osteomyelitis.[1]

The radiographic appearance of fibrous dysplasia lesions may be protean and, hence, can appear in a differential diagnosis for lesions that may vary in appearance from lytic to densely sclerotic. Most commonly, fibrous dysplasia lesions initially demonstrate a purely lytic appearance and then develop a hazy or "ground glass" appearance as the matrix calcifies. Such lesions tend to occur centrally within bone, vs. being cortically based, and often have an expansile appearance. Fibrous dysplasia may present in monostotic (80% to 85%) or polyostotic (15% to 20%) patterns. Bone scan is useful for evaluating polyostotic disease since the lesions usually demonstrate increased activity. Uptake in a lesion that is out of proportion to other lesions in polyostotic fibrous dysplasia can indicate a complication, such as pathologic fracture or a synchronous lesion of a different etiology, such as infection or malignancy. When polyostotic, fibrous dysplasia lesions are often unilateral, most commonly found in the femur, tibia and pelvis.[2] Several syndromes are associated with polyostotic fibrous dysplasia. McCune-Albright syndrome includes the triad of polyostotic fibrous dysplasia, precocious puberty and café-au-lait spots (coast of Maine). Mazabraud syndrome is defined by polyostotic fibrous dysplasia and multiple soft tissue myxomas. Clinically, fibrous dysplasia lesions are not painful unless complicated by pathologic fracture.

NOF (often used synonymously with fibrous cortical defect or fibroxanthoma) is a common lesion in the pediatric population with incidences reported as high as 20%. Most of these lesions spontaneously regress in early adulthood and, thus, go undetected unless found incidentally. The radiographic appearance of NOF is pathognomonic and may be described as cortically based, somewhat expansile, and perhaps with a thin, scalloped, sclerotic border. Such lesions are typically seen within the metaphysis of long bones, often about the knee. Like fibrous dysplasia, NOF is not associated with periosteal reaction and is not painful unless complicated by trauma. Bone scintigraphy may reveal increased uptake, ie, a "hot" appearance, during the "healing phase" of these lesions secondary to increased osteoblastic activity.[3] This activity should not prompt concern for a more aggressive etiology in the absence of concerning imaging findings, as the diagnosis can typically be made with imaging findings alone. Biopsy should be avoided as these lesions may reveal a more aggressive histopathological appearance resulting in unnecessary treatment-related morbidity.[4]

LCH, like fibrous dysplasia, often presents radiographically in a protean manner. Lesions may be lytic or sclerotic and may have well-defined sclerotic margins vs. ill-defined borders. Unlike fibrous dysplasia or NOF, however, LCH lesions may have a periosteal reaction and exhibit a more aggressive appearance.[5] A bony sequestrum may be associated with this lesion. LCH lesions may or may not be associated with pain and are encountered nearly exclusively in the pediatric and young adult population.[5] LCH is most commonly monostotic, but may be polyostotic. Bone scan is useful for identifying polyostotic disease, although it needs to be used in conjunction with radiography as uptake is variable depending on histology, and the modalities have overlapping false negatives.[6] However, uptake on bone scintigraphy indicates active disease, making it useful to clinicians, particularly when evaluating for treatment response.

Osteomyelitis can affect any bone in any patient. Bone infection can have a wide range of radiographic presentations from a highly aggressive appearance with periosteal reaction, to a benign appearance with well-defined sclerotic margins.[7] Osteomyelitis can appear expansile and may obliterate fat planes, invariably resulting in effusions or cartilage loss if the process involves a joint.[7] A bony sequestrum is common in osteomyelitis. The benign appearance can be seen particularly when osteomyelitis is subacute or chronic, as well as with chronic recurrent multifocal osteomyelitis, an idiopathic inflammatory disorder primarily seen in the pediatric population.[8] Osteomyelitis instigates an osteoblastic response and, therefore, demonstrates increased uptake on bone scan. Bone scan uptake can be seen up to 14 days prior to radiographic findings.[9] A three-phase positive bone scan, meaning increased activity on dynamic flow, immediate static blood pool, and delayed static images, is 73% to 100% sensitive for osteomyelitis.[10] A negative three-phase bone scan essentially excludes osteomyelitis.

Diagnosis

Polyostotic fibrous dysplasia

Patient Follow-Up

The patient was treated with curettage and grafting of the proximal femoral lesion with plating of the pathologic fracture. The entire femur was stabilized with intramedullary rods due to the presence of additional lesions. Histopathology confirmed a diagnosis of fibrous dysplasia. The patient was identified as having a G-protein defect, which is specific

for McCune-Albright syndrome. Despite having polyostotic fibrous dysplasia and McCune-Albright specific G-protein defect, the diagnosis of McCune-Albright syndrome was deferred as the patient did not have laboratory or physical exam findings consistent with precocious puberty or café-au-lait spots, other components of the McCune-Albright syndrome.

Summary

Nonaggressive-appearing bone lesions (well-defined margins, narrow zone of transition, lack of periosteal reaction) are often incidental findings in the pediatric population. These lesions are typically asymptomatic unless complicated by trauma/pathologic fracture, the other circumstance under which they are typically found. Radiography is the imaging modality most often used for initial evaluation. CT, MRI, and bone scintigraphy are also helpful for further characterization. Laboratory testing is useful if osteomyelitis is suspected or the process is polyostotic. Genetic testing may be indicated for the evaluation of polyostotic bone lesions secondary to syndromic etiologies.

References

1. Levine SM, Lambaise RE, Petchprapa CN. Cortical lesions of the tibia: characteristic appearances at conventional radiography. Radiographics 2003;23:157-177.
2. Fitzpatrick KA, Talijanovic MS, Speer DP, et al. Imaging findings of fibrous dysplasia with histopathology and intraoperative correlate. Am J Roentgenol 2004;182:1389-1398.
3. Machida K, Makita K, Nishikawa J, et al. Scintographic manifestation of fibrous dysplasia. Clin Nucl Med 1986;11:426-429.
4. Betsy M, Kupersmith LM, Springfield DS. Metaphyseal fibrous defects. J Am Acad Orthop Surg 2004;12:89-95.
5. Kilborn TN, The J, Goodman TR. Paediatric manifestations of Langerhans cell histiocytosis: a review of the clinical and radiological findings. Clin Radiol 2003;58:269-278.
6. Azouz EM, Saigal G, Rodriguez MM, et al. Langerhans' cell histiocytosis: pathology, imaging and treatment of skeletal involvement. Pediatr Radiol 2005;35(2):103-115.
7. Blickman JG, van Die CC, de Rooy JWJ. Current imaging concepts in pediatric osteomyelitis. Eur Radiol Suppl 2004;14:L55-L64.
8. Khanna G, Sato TS, Ferguson P. Imaging of chronic recurrent multifocal osteomyelitis. Radiographics 2009;29(4):1159-1177.
9. Schauwecker DS. The scintigraphic diagnosis of osteomyelitis. Am J Roentgenol 1992;158(1):9-18.
10. Pineda C, Vargas A, Rodriguez AZ. Imaging of osteomyelitis: current concepts. Infect Dis Clin North Am 2006;20(4):789-825.

Disclaimer: *The views expressed in this article are those of the author and do not necessarily reflect the official policy or position of the Department of the Navy, Department of Defense, or the U.S. Government.*

JAOCR at the Viewbox

Brendon G. Tillman, M.D., Mickaila J. Johnston, M.D.

Department of Radiology, Naval Medical Center San Diego, San Diego, CA

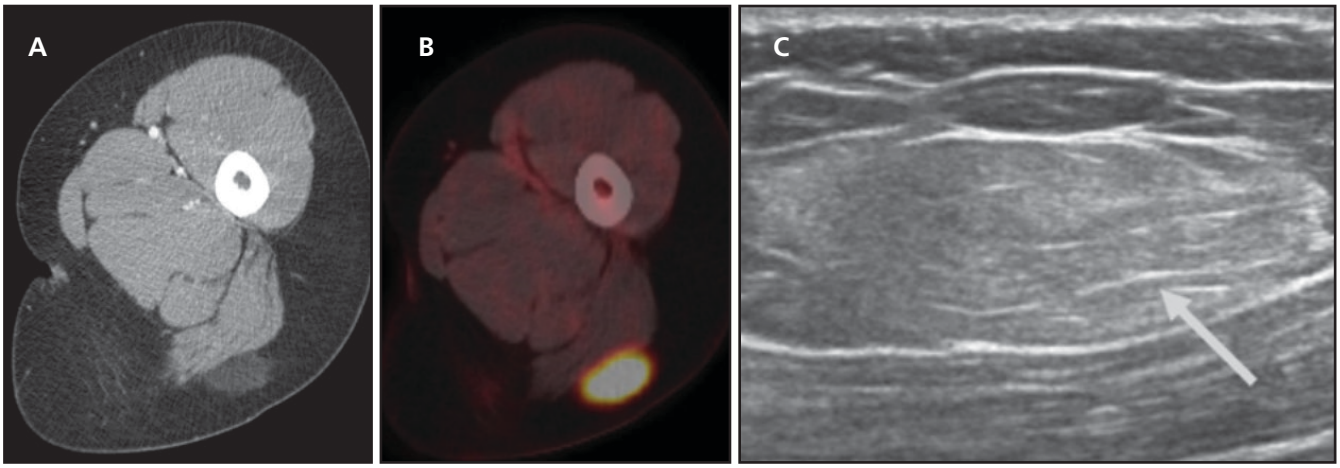

Hibernoma

A 26-year-old woman with multiple endocrine neoplasia type 1 (MEN1) was referred for positron emission tomography-computed tomography (PET-CT) to evaluate a new pancreatic mass. Axial CT (A) and fused PET-CT (B) images show an ovoid hypermetabolic low-density lesion in the subcutaneous fat of the left thigh, abutting the posterior muscular compartment. Subsequent ultrasound shows the lesion to be hyperechoic (C, arrow). Differential considerations included hibernoma, liposarcoma, atypical lipoma, and metastases. Ultrasound-guided biopsy revealed a hibernoma.

Hibernomas are rare, benign brown adipose-containing tumors typically in intramuscular fatty regions. The 4 types, from most to least common, are: typical, myxoid, lipoma-like, and spindle cell.[1] Approximately 30% are located in the thigh, followed by the shoulder and back. Mutations involving the chromosome band 11q13 are linked to hibernomas and MEN1 syndrome, with several case reports demonstrating a possible link.[2]

Hibernomas typically have attenuation between fat and muscle with varying degrees of enhancement.[2] On ultrasound, hibernomas are usually well-delineated and hyperechoic, similar to lipomas. They are intensely fluorine 18 fluorodeoxyglucose (FDG)-avid and have signal intensity similar to fat on MR. Imaging is not diagnostic. Percutaneous biopsy can be helpful, but surgical excision is usually recommended.

References

1. Murphey MD, Carrol JF, Flemming DJ, et al. From the archives of the AFIP: benign musculoskeletal lipomatous lesions. *Radiographics* 2004;24(5):1433-1466.
2. Daubner D, Spieth S, Pablik J, et al. Hibernoma – two patients with a rare lipoid soft-tissue tumour. *BMC Med Imaging* 2015;15:4.

Disclaimer: The views expressed in this article are those of the author and do not necessarily reflect the official policy or position of the Department of the Navy, Department of Defense, or the U.S. Government.

JAOCR at the Viewbox

Mickaila J. Johnston, M.D., Michael Starsiak, M.D.

Department of Radiology, Naval Medical Center San Diego, San Diego, CA

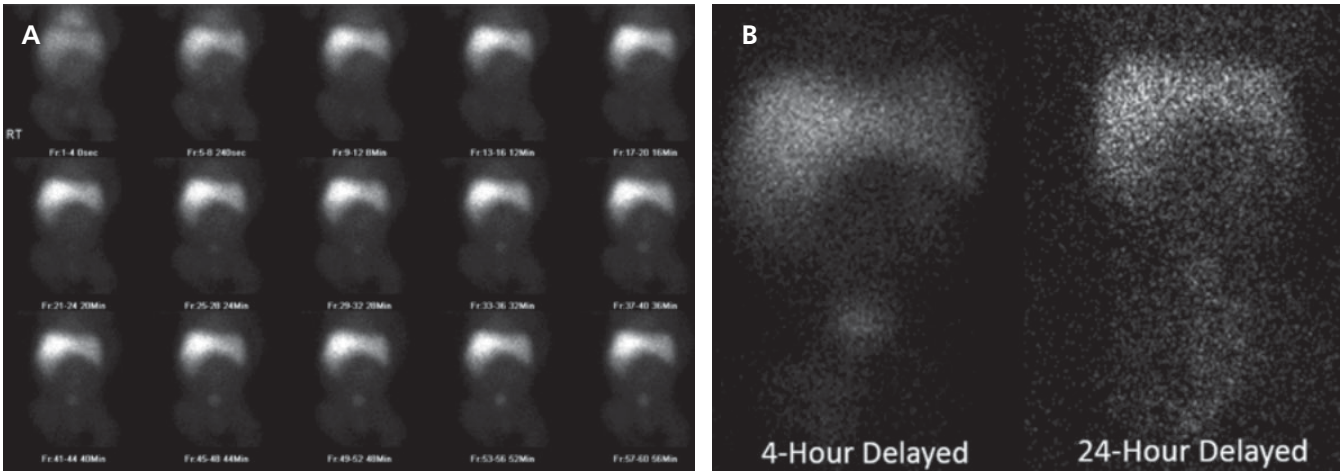

Biliary Atresia

A 38-day-old boy was referred for evaluation of acholic stools and elevated direct hyperbilirubinemia. After 4 days of intravenous phenobarbital administration, a Tc99m-mebrofenin hepatobiliary scan was obtained. Sixty-minute dynamic imaging revealed blood pool clearance of radiotracer and concentration within the liver, but no transit of radiotracer to the gallbladder or bowel (A). Delayed static imaging at 4 and 24 hours (B) revealed a persistent hepatogram and no transit of radiotracer to the bowel or gallbladder. Incidental vicarious genitourinary clearance was noted, which can be seen with elevated bilirubin levels.

Differential considerations for a persistent hepatogram with lack of transit to the gallbladder or bowel on delayed images in an infant include biliary atresia, immature intrahepatic transport mechanisms, and inappropriate (or lack of) pretreatment with anti-cholestatic medication. Similar hepatobiliary scan findings can be seen with complete obstruction of the common bile duct, chronic partial obstruction of the common bile duct, pancreatitis, severe concomitant illness, and hepatocellular disease.

Extrahepatic biliary atresia may present as prolonged jaundice, acholic stool, dark urine, failure to thrive, and/or hepatomegaly. Early corrective surgery, most often with Kasai portoenterostomy, is desired. Subsequent liver transplant later in life may be necessary. Barshes et al demonstrated a 10-year actuarial survival rate of 85.8% in 1,976 patients undergoing liver transplant for biliary atresia from 1988-2003.[1]

Reference

1.Barshes NR, Lee TC, Balkrishan R, et al. Orthotopic liver transplantation for biliary atresia: the U.S. experience. Liver Transpl 2005;11(10):1193-1200.

Disclaimer: The views expressed in this article are those of the author and do not necessarily reflect the official policy or position of the Department of the Navy, Department of Defense, or the U.S. Government.